Generalized exceptional points in nonlinear and stochastic dynamics

Cheyne Weis,[1] Michel Fruchart,[1,2] Ryo Hanai [3] Kyle Kawagoe [1,4,5] Peter B. Littlewood,[1,6] and Vincenzo Vitelli [1,4]

[1]*James Franck Institute and Department of Physics, The University of Chicago, Chicago, Illinois 60637, USA*
[2]*Gulliver, UMR CNRS 7083, ESPCI Paris PSL, 75005 Paris, France*
[3]*Department of Physics, Institute of Science Tokyo, 2-12-1 Ookayama Meguro-ku, Tokyo 152-8551, Japan*
[4]*Leinweber Institute for Theoretical Physics, The University of Chicago, Chicago, Illinois 60637, USA*
[5]*Department of Physics and Department of Mathematics, The Ohio State University, Columbus, Ohio 43210, USA*
[6]*School of Physics and Astronomy, University of St Andrews, St. Andrews KY16 9AX, United Kingdom*

We study a class of bifurcations generically occurring in dynamical systems with nonmutual couplings ranging from models of coupled neurons to predator-prey systems and nonlinear oscillators. In these bifurcations, extended attractors such as limit cycles, limit tori, and strange attractors merge and split in a similar way as fixed points in a pitchfork bifurcation. We show that this merging and splitting coincide with the coalescence of covariant Lyapunov vectors with vanishing Lyapunov exponents, a feature that generalizes the exceptional points that can exist in families of non-Hermitian matrices or operators. We distinguish two classes of bifurcations associated with generalized exceptional points, corresponding respectively to continuous and discontinuous behaviors of the covariant Lyapunov vectors at the transition depending on the presence of a $\mathbb{Z}_2$ symmetry. We outline some physical consequences of this class of theories exhibiting generalized exceptional points, including nonreciprocal responses, the destruction of isochrons, and anomalous noise effects. In particular, we show that the effective diffusion coefficient on the attractor can stay finite or even diverge when the noise strength vanishes. We illustrate our results with concrete examples from neuroscience, ecology, and physics.

I. INTRODUCTION

The dynamics of linear systems is summarized by their so-called normal modes, and the corresponding oscillation frequencies and decay rates. These are the eigenmodes and eigenvalues of the linear operator (dynamical matrix or Hamiltonian) describing the system. Open systems are often described by non-Hermitian operators, or in simpler cases real-valued asymmetric matrices [1–6]. These mathematically capture dissipation and active driving, as well as the possible nonmutual (or nonreciprocal) couplings between the relevant degrees of freedom or fields (i.e., the action of A on B is different from the action of B on A). Of special interest are points in parameter space where such operators or matrices become nondiagonalizable and at least two eigenvectors coalesce—they are technically known as exceptional points [2,7]. Despite their name, exceptional points are rather common: a harmonic oscillator at critical damping is a simple example [[8], Sec. 25]. Exceptional points typically mark the transition between traveling or oscillatory solutions and exponentially growing/decaying dynamics. In linear systems, exceptional points possess distinctive properties [1,4,9–14] including an enhanced sensitivity to perturbations [10] as well as chiral mode conversion when dynamically encircling the

exceptional point [9,15–17]. It is not clear to what extent these properties extend to nonlinear systems. Indeed, nonlinearities are often crucial in nonreciprocal systems since the linearized dynamics of these driven, active or excitable media can be unstable, leading to phase transitions between time-dependent states. The study of these transitions is tantamount to investigating bifurcations of the underlying dynamical system [18–24].

One of the simplest examples of a bifurcation is an elastic beam buckling under a load [18,25]. The vertical beam is straight below a critical load at which it can curve either to the left or to the right. Mathematically, this phenomenon is described by a pitchfork bifurcation [Fig. 1(a)]: it describes the appearance of the left- and right-buckled state of the beam that bifurcate from the unbuckled state at the critical load. In the pitchfork bifurcation, the steady states of the system are fixed points. The unbuckled state is symmetric with respect to left-right inversion, while the buckled states break this symmetry, and therefore occur in conjugate pairs that coalesce at the bifurcation point.

In this article, we analyze certain classes of bifurcations in which the states coalescing at the bifurcation point are dynamical steady states (called attractors) as opposed to the two fixed points corresponding to the static shapes of the buckled beam. These coalescing steady states can be limit cycles [closed orbits corresponding to a periodic evolution in time; see Fig. 1(b)], limit tori, or strange attractors [more complicated structures that generally correspond to a chaotic evolution; see Fig. 1(c)]. The underlying dynamical systems need not possess any symmetry besides time-translation invariance, i.e.,

(a)

(b)

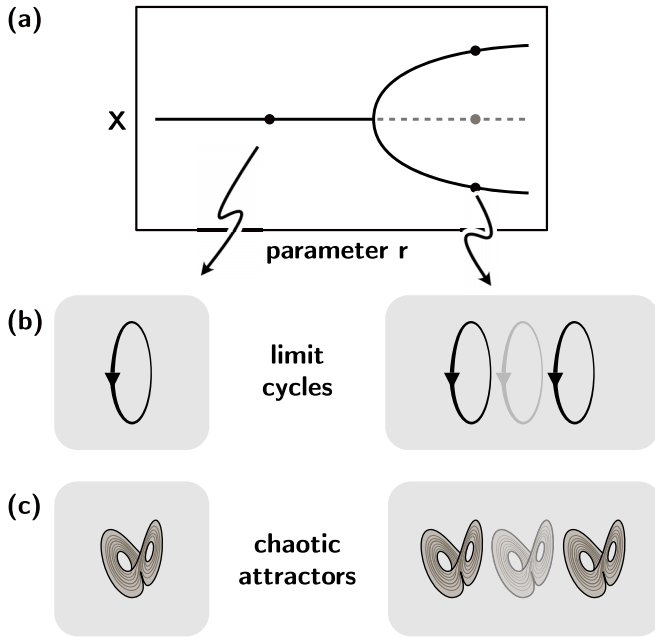limit
cycles

(c)

chaotic
attractors

FIG. 1. Pitchfork bifurcation of attractors and Lyapunov vectors. In a pitchfork bifurcation (a), a stable fixed point bifurcates into an unstable fixed point (dashed line) plus two stable fixed points when a control parameter r reaches a critical value. This can be extended to generic attractors, such as limit cycles (b), higher-dimensional tori, or chaotic attractors (c), in which unstable attractors (repellers) are drawn with a lower opacity.

they need not be equivariant under a continuous symmetry group, unlike the cases considered in [26] and references therein. We show that the coalescence of attractors is accompanied by a generalized exceptional point defined in terms of so-called Lyapunov exponents and covariant Lyapunov vectors [27,28], that serve as generalized normal modes. The generalized exceptional point we investigate is an exact tangency of two covariant Lyapunov vectors with vanishing Lyapunov exponents (see Appendix E for the case of finite Lyapunov exponents). These mathematical objects capture the dynamics of perturbations around the attractor, generalizing to extended attractors of nonlinear systems the notion of exceptional points familiar from linear non-Hermitian physics.

This mathematical approach allows one to explore the rich phenomenology that arises as a result of this coalescence of attractors across various domains of science. In the remainder of this paper, we develop a general theory for the coalescence of dynamical attractors in nonreciprocal dynamical systems based on the behavior of the covariant Lyapunov vectors at the bifurcation. Next, we explore consequences of the combination of generalized exceptional points with noise or external perturbations. We illustrate this behavior in several different physical models describing predator-prey systems, neural dynamics, coupled Hopf oscillators and chaotic dynamics. Finally, we highlight how our analysis can be used to explain existing experimental observations ranging from plankton dynamics [29] to stochastic rotation reversals of rigid bodies in convection cells [30].

II. GENERALIZED EXCEPTIONAL POINTS IN NONLINEAR DYNAMICS

A. Linearized dynamics and exceptional points

Start with a dynamical system

$$\dot{X} = f(X) \qquad (1)$$

in which $X(t) \in \mathbb{R}^N$ is a vector (the dot represents the time derivative, and f is a function $\mathbb{R}^N \to \mathbb{R}^N$ defining the dynamical system). Consider now two nearby states that evolve by following the same dynamical system. At long times, will these states be closer or farther away?

Around a fixed point X_0 of the dynamical system, defined by $f(X_0) = 0$, the answer is given by the Jacobian

$$J_{ab} = \frac{\partial f_a}{\partial X_b} \qquad (2)$$

evaluated at the fixed point X_0 of interest. The difference $\delta X(t)$ between the perturbed trajectory and the unperturbed one [31] evolves according to

$$\delta \dot{X} = J \delta X. \qquad (3)$$

Hence, perturbations along the eigenvector c_i of J with eigenvalue $\lambda_i + i\omega_i$ grows or decays as $e^{\lambda_i t}$.

To draw this conclusion, we have implicitly assumed that the Jacobian J can be diagonalized. However, not all matrices are diagonalizable: a counterexample is the nondiagonalizable matrix

$$J_{\text{EP}} \equiv \begin{pmatrix} 0 & 1 \\ 0 & 0 \end{pmatrix}. \qquad (4)$$

These matrices are somewhat unusual: they typically occur at codimension-two points in parameter space called exceptional points [7] (for instance, they would be isolated points in a two-dimensional parameter space [32]). The particular form in Eq. (4) is called a Jordan block [33]. Despite occurring at isolated points, these nondiagonalizable matrices do play an important role when they appear in the description of a physical or biological system.

Physically, the main feature of the matrix Eq. (4) is that it encodes a nonreciprocal interaction between the two degrees of freedom (i.e., vector components) on which it operates: as $J_{12} = 1$, the degree of freedom 2 has an effect on 1, while 1 has no effect on 2 because $J_{21} = 0$. Mathematically, a crucial feature of this matrix is that it is nonnormal [10]. A matrix M is normal when it is unitarily diagonalizable. In contrast, nonnormal matrices can have nonorthogonal eigenvectors. In fact, when one approaches an exceptional point in parameter space, two eigenvectors of the matrix become more and more collinear, and end up parallel to each other at the exceptional point, like c_i and c_j in Fig. 2(b) (middle).

In the context of dynamical systems, the nondiagonalizable matrix Eq. (4) appears as (a block in) the Jacobian of dynamical systems undergoing a so-called Bogdanov-Takens bifurcation [34]. This is a codimension-two bifurcation that occurs in systems ranging from fluid mechanics to ecology and neuroscience [34–37]. It can be seen as the intersection of a Hopf bifurcation and a saddle-node bifurcation.

Deviations from normality produce striking physical consequences related to transient growths and to an enhanced
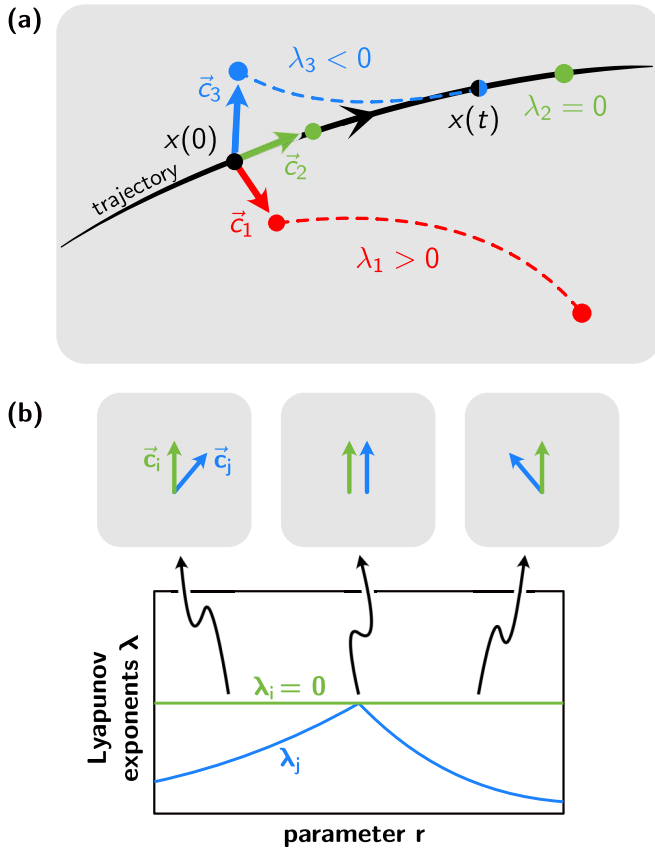
FIG. 2. Coalescence of Lyapunov exponents and covariant vectors at the bifurcation. In panel (a), we provide a schematic picture of Lyapunov exponents λ_i and (covariant) Lyapunov vectors c_i. Consider an initial condition $x(0)$ for a dynamical system $\dot{x} = f(x)$. It evolves into $x(t)$. A slightly perturbed initial condition $x(0) + \epsilon \delta x$ ($\epsilon \ll 1$) evolves under the same dynamical system. Decomposing the perturbation δx over the covariant Lyapunov vectors $c_i(0)$, we can predict whether at long times, the perturbation will grow ($\lambda > 0$, red), decay ($\lambda < 0$, blue), or stay finite ($\lambda = 0$, green). In panel (b), we show the evolution of Lyapunov exponents and covariant Lyapunov vectors through the bifurcation represented in Fig. 1(a). One Lyapunov exponent λ_i, corresponding to the motion along the attractor c_j, always vanishes. At the transition, another Lyapunov exponent λ_j goes to zero, while the corresponding Lyapunov vector c_j becomes parallel to c_i.

sensitivity to fluctuations and to boundary conditions [1,2,4,10,38–40]. For instance, consider an initial perturbation $\delta X(0) = (\delta X_1^0, \delta X_2^0)$ evolving according to Eq. (3) with the Jacobian $J = J_{\text{EP}}$ in Eq. (4). Based on the (vanishing) eigenvalues of J_{EP} alone, one may expect that the perturbation will have a constant magnitude. Yet an explicit solution

$$\delta X(t) = \begin{pmatrix} X_1^0 + X_2^0 t \\ X_2^0 \end{pmatrix} \tag{5}$$

shows that δX actually growth with time, until the anomalous polynomial growths $\delta X_1(t) \sim X_2^0 t$ is stopped by nonlinearities. When the eigenvalue λ associated to the Jordan block is finite and negative ($J = J_{\text{EP}} + \lambda \text{Id}$ with $\lambda < 0$), the polynomial growth observed above still takes place, but it is eventually stopped by an exponential prefactor $e^{\lambda t}$. In addition

to the polynomial growth, note that a perturbation initially along the direction δX_2 gradually moves along direction δX_1. The converse does not occur: perturbations along δX_1 stay along this direction. This is nonreciprocity in action. Both the anomalous growth and the nonreciprocal evolution of perturbations arise not only at exceptional points, but also in their neighborhood, where the Jacobian is strongly nonnormal.

B. Lyapunov exponents and covariant Lyapunov vectors

When the dynamical system has attractors with a spatial extent in configuration space (like a limit cycle), the Jacobian at a single point is insufficient to indicate if the system has the characteristics of an exceptional point [41]. As before, perturbations δX about an unperturbed trajectory $X_0(t)$ evolve according to

$$\delta \dot{X} = J(X_0(t)) \delta X. \tag{6}$$

in which the Jacobian now depends on time through the unperturbed trajectory $X_0(t)$.

Formally, this linear differential equation is solved by defining the evolution operator as the time-ordered exponential [42]

$$U(t, t_0) = T \exp\left(\int_{t_0}^t J(X_0(\tau)) d\tau \right), \tag{7}$$

very much like in quantum mechanics [43,44]. Most of the time (see next Sec. II C for the exception), the evolution operator can thus be decomposed as

$$U(t, t_0) = \sum_i |c_i(t)\rangle\, e^{\int_{t_0}^t \lambda_i(\tau) d\tau}\, \langle \tilde{c}_i(t_0)|, \tag{8}$$

in which $c_i(t)$ are called covariant Lyapunov vectors (CLVs), $\lambda_i(t')$ are instantaneous growth rates associated to the CLVs, and $\tilde{c}_i$ are called dual (or adjoint) CLVs [27,45]. The function $U(t; X_0)$ (where we have dropped $t_0 = 0$ to simplify and made the dependence on X_0 explicit) satisfies the group relation $U(t + s; X) = U(t + s; \Phi^t X) U(s; X)$ in which Φ^t is the flow of the dynamical system (1), that propagates an initial condition $X(0) = X_0$ to later times as $X(t) = \Phi^t X_0$. This means that it is a cocycle, known as the Lyapunov-Oseledets cocycle [46,47]. At long times, the time averages of the instantaneous growth rates converge towards the Lyapunov exponents

$$\lambda_i = \lim_{t \to \infty} \frac{1}{t} \int_0^t \lambda_i(t') dt'. \tag{9}$$

The decomposition corresponding to (8) is known as an Oseledets splitting. We emphasize that the CLVs are not necessarily orthogonal to each other [namely, $\langle c_i(t), c_j(t)\rangle \neq \delta_{ij}$]. The dual CLVs generalize left eigenvectors, while normal CLVs generalize right eigenvectors, so $\langle \tilde{c}_i(t), c_j(t)\rangle = \delta_{ij}$.

An arbitrary perturbation $\delta X(0)$ at time $t = 0$ then evolves as [46,48]

$$\delta X(t) = U(t, 0) \delta X(0) = \sum_i a_i e^{\int_0^t \lambda_i(t') dt'} c_i(t) \tag{10}$$

in which the a_i are the coefficients obtained by projecting the initial perturbation $\delta X(0)$ on the CLVs $c_i(0)$. Infinitesimal perturbations either decay exponential ($\lambda_i < 0$), grow exponentially ($\lambda_i > 0$), or stay constant ($\lambda_i = 0$) at long times, as

illustrated in Fig. 2(a). Perturbations along the covariant Lyapunov vector c_i grow or decay with the Lyapunov exponent λ_i [Fig. 2(a)]. The Lyapunov exponents generalize the (real part of the) eigenvalues of the Jacobian at a fixed point, while the covariant Lyapunov vectors generalize the eigenvectors [49]. For more details about Lyapunov exponents and covariant Lyapunov vectors and applications, we refer the readers to Refs. [27,28,45,47,50–60]. Please note that the CLVs $c_i(t)$ depend on time, because they have to follow the unperturbed trajectory. Indeed, most of the complexity of the time evolution Eq. (6) is crucially packed into the time dependence of the CLVs.

Although CLVs are generically nonorthogonal, the normalization of the vectors can often be chosen such that $\langle \tilde{c}_i, c_j \rangle = \delta_{ij}$. Doing so is *almost* always possible: the only exception are generalized exceptional points, that we discuss in the next section.

C. Generalized exceptional points

Equations (10) and (8) are valid most of the time, but not always. Indeed, Eq. (7) must encompass the simple example of a constant nondiagonalizable Jacobian such as Eq. (4), for which Eqs. (10) and (8) do not apply as is. This feature can extend to nonconstant Jacobians. In general, one has to write

$$U(t, t_0) = \sum_{ij} |c_i(t)\rangle \, \Lambda_{ij}(t) \, \langle \tilde{c}_j(t_0)| \tag{11}$$

in which $\Lambda_{ij}(t)$ is composed of Jordan blocks, and hence is not necessarily diagonal [61,62]. This situation is the generalization of an exceptional point. It occurs when two Lyapunov exponents are equal and the corresponding CLVs, say, $c_1(t)$ and $c_2(t)$, become identical [Fig. 2(b)] [63]. At the singularity, the evolution operator cannot be diagonalized anymore and assumes a Jordan block form. In the simplest case of a Jordan block of size two [64],

$$\Lambda(t) \simeq \begin{pmatrix} \Lambda_1(t) & \Lambda_{12}(t) \\ 0 & \Lambda_1(t) \end{pmatrix}, \tag{12}$$

where $\Lambda_1(t) = e^{\int_{t_0}^{t} \lambda_1(\tau) d\tau}$. This can be seen as a generalization of Eq. (4). Applying a similarity transformation $J \mapsto P^{-1}JP$ (with an arbitrary invertible matrix P) leaves the matrix J in Eq. (4) nondiagonalizable. Similarly, the presence of a generalized exceptional point where two CLVs are parallel is invariant under a nonlinear change of coordinate of the dynamical system (see Appendix B of Ref. [53] for how CLVs transform under such a change of coordinates). Because of the covariance of the CLVs with respect to the time evolution, two CLVs that are exactly parallel at one point of the trajectory remain exactly parallel all along the trajectory [65]. We refer to [61] for a discussion in terms of the Lyapunov-Oseledets cocycle.

The case in which two CLVs are almost identical has been known as *near tangencies* in the literature [45,66–71]. In this work, we focus on *exact* tangencies (i.e., generalized exceptional points). It is natural to expect near tangencies in the neighborhood of generalized tangencies. This is indeed what we observe in several cases. As we shall see, this does not always happen: perhaps surprisingly, the behavior of CLVs can be discontinuous.

1. Generalized EPs with vanishing Lyapunov exponent

The main focus of this work is the case of exact tangencies (generalized EPs) where the involved CLVs have vanishing Lyapunov exponents. These tangencies correspond to bifurcations in the underlying dynamical system.

We have implicitly assumed that the dynamical system in Eq. (1) is autonomous, namely, that f does not explicitly depend on time. As a consequence, the dynamical system Eq. (1) always has a vanishing (local and global) Lyapunov exponent $\lambda_* = 0$ corresponding to the CLV $\vec{c}_* \equiv f$ tangent to the trajectory at each point [27]. This can be shown directly by taking the time derivative of Eq. (1) and using the chain rule, yielding $(d/dt)\dot{X} = J(X(t))\dot{X}$ from which one can show that the corresponding Lyapunov exponent must vanish, provided that the vector field f is not singular [[27], Sec. 2.5.6]. One can interpret this fact as a consequence of the time-translation invariance of the dynamical system, that is spontaneously broken by the solutions.

2. Generalized EPs with finite Lyapunov exponent

It is also possible to find tangencies between CLVs with finite Lyapunov exponents that coincide with a change in the transient behavior of the system rather than a change in the nature of the attractors. In other words, they do not correspond to a bifurcation of the dynamical system. A finite Lyapunov exponent CLV tangency can be demonstrated in a linear system $\dot{x} = Ax$ with a fixed point [72]. When a parameter is tuned such that two eigenvalues of A coalesce at a finite value to become a complex conjugate pair, the fixed point will change from a node to a focus changing the transient dynamics. Other examples are discussed in Appendix E.

III. COALESCENCE OF ATTRACTORS AND GENERALIZED EXCEPTIONAL POINTS

A. Parity-breaking bifurcations

As a first example, consider the so-called parity-breaking bifurcation [73]

$$\dot{\phi} = w, \tag{13a}$$

$$\dot{w} = rw - w^3. \tag{13b}$$

The variable ϕ can be seen as an angular variable representing the motion of a point on a circle of fixed radius, or as a real variable representing the motion of a point on the line [74]. The variable w is an additional variable that undergoes a pitchfork bifurcation when the parameter r changes sign (neither w nor r are related to the radius of the circle). At the same time, the full dynamical system (13) undergoes a parity-breaking bifurcation (also known as drift-pitchfork bifurcation). This bifurcation occurs in pattern formation [75–81], fluid dynamics [82,83], excitable media [84,85], coupled lasers [86–88], synchronization [26,89–91], biological tissues [92], driven-dissipative condensates [93,94], active matter and other collective phenomena [26,95–98]. When $r < 0$, ϕ is constant, so the system simply has a circle of fixed points corresponding to all the possible values of ϕ (heuristically, this can be visualized as a limit cycle with a vanishing frequency of oscillation). When $r > 0$, a limit cycle appears.

The frequency $\pm\sqrt{r}$ has a sign that is determined by the sign of the initial condition $\mathrm{sgn}[w(t=0)]$. Hence, the sense of rotation (clockwise or counterclockwise) of the limit cycle in the parity-breaking bifurcation is not determined in advance: it depends on the initial conditions. This is in contrast with the case of a Hopf bifurcation, in which the sense of rotation is always the same for a given set of parameters.

Let us compute the Jacobian of the dynamical system defined by Eq. (13). Evaluated at $w=0$, it is

$$J = \begin{pmatrix} 0 & 1 \\ 0 & r \end{pmatrix}. \tag{14}$$

This matrix becomes nondiagonalizable at the bifurcation point $r=0$. In other words, the bifurcation occurs at an exceptional point of the Jacobian [99].

B. Pitchfork of attractors

The parity-breaking bifurcation introduced in the previous paragraph describes a transition from a stable circle of fixed points to two limit cycles (plus an unstable circle of fixed points). In a rotating frame of reference, this is equivalent to a bifurcation from a single limit cycle to two different limit cycles (plus an unstable limit cycle). This suggests that a generalized notion of exceptional point could appear when the Jacobian is not constant along trajectories, even if it is difficult or impossible to do the equivalent of rotating the reference frame. This could occur for limit cycles, but also more complex attractors. In order to analyze this situation, we generalize Eq. (13) to produce a pitchfork of attractors in which a given nonlinear attractor splits or merges into attractors of the same nature.

We start with a dynamical system producing the desired attractor, of the form

$$\dot{x} = f(x) \tag{15}$$

in which $x \in R^M$. This dynamical system is controlled by a 1D system exhibiting a pitchfork bifurcation as follows:

$$\dot{x} = f(x) + g(x, w), \tag{16a}$$
$$\dot{w} = rw - w^3. \tag{16b}$$

The simplest coupling consists in making the parameters of f depend on the value of w (a bit like in a parametric oscillator) [100]. The properties of the attractor described by f are then tuned through w. Because there are two possible (stable) values of w on the right of the pitchfork bifurcation, there are also two different attractors, whose properties gradually become identical when we approach the pitchfork bifurcation.

C. Pitchfork of limit cycles

Let us illustrate these ideas when f is the normal form of a Hopf oscillator. In this case, it is convenient to write $x = (x_1, x_2)$ as a complex number $z = x_1 + i x_2$, and the general form Eq. (16) becomes

$$\dot{z} = (\alpha + \beta |z|^2) z + \gamma h(w) z, \tag{17a}$$
$$\dot{w} = rw - w^3, \tag{17b}$$

where α, β, γ are complex, while r and the arbitrary function $h(w)$ are real. Here adding the coupling $g(z, w) = \gamma h(w) z$

is equivalent to replacing the coupling α with $\alpha'(w) = \alpha + \gamma h(w)$. Let us analyze the dynamical system Eq. (17). First, Eq. (17b) shows that $w = 0$ when $r < 0$ and $w = \pm\sqrt{r}$ when $r > 0$, irrespective of the value of z. Then, writing $z = R(t)e^{i\phi(t)}$ and $\alpha = \alpha_r + i\alpha_i$ (similar for α', β, and γ), we find that

$$\dot{R} = \alpha'_r R + \beta_r R^3, \tag{18a}$$
$$\dot{\phi} = \alpha'_i + \beta_i R^2. \tag{18b}$$

Hence, a limit cycle with radius $R = \sqrt{-\alpha'_r(w)/\beta_r}$ and angular frequency $\Omega = \alpha'_i(w) - \beta_i/\beta_r \alpha'_r(w)$ exists when the inside of the square root is positive (the period of the oscillation is $T = 2\pi/\Omega$). Otherwise, there is a stable fixed point $R = 0$. The radius and frequency of the limit cycle depend explicitly on w. Hence, on the symmetry-breaking side of the pitchfork bifurcation ($r > 0$), there are two different limit cycles whose properties depend on the value of $w = \pm\sqrt{r}$, provided that $h(w) \neq h(-w)$. The system mimics a traditional pitchfork bifurcation, but with stable/unstable fixed points replaced with stable/unstable limit cycles. Let us tune the parameters of the Hopf bifurcation so that a stable limit cycle exists [101]. For $r < 0$, there is a single limit cycle invariant under the transformation $w \rightarrow -w$. For $r > 0$, there are two stable limit cycles that are mapped to each other by the transformation $w \rightarrow -w$, plus an unstable cycle that is mapped onto itself. (We refer to Appendix B for a discussion on symmetries.) At $r = 0$, a pitchfork bifurcation of limit cycles occurs (see also Refs. [34,102–104] and for examples Refs. [105–111]), in which the two stable limit cycles and the unstable one merge into one stable cycle, as depicted in Fig. 3(c). In this bifurcation, the radius of the limit cycle is irrelevant. Therefore, it can be ignored to focus on the reduced dynamics

$$\dot{\phi} = \omega_0 + \omega_1 w, \tag{19a}$$
$$\dot{w} = rw - w^3. \tag{19b}$$

similar to Eq. (13). As the bifurcation is approached, the limit cycles are pushed against each other, the distance between the cycles shrinks. One can expect that this confinement may constrain the dynamics of small perturbations close to the attractors to be tangent to the cycles. As we now show, this expectation can be made precise using Lyapunov exponents and covariant vectors.

In the case of limit cycles, the Lyapunov exponents and covariant vectors can be computed using Floquet theory. More precisely, the real part of the Floquet exponents are the Lyapunov exponents, while the corresponding Floquet eigenvectors span the same spaces as the covariant Lyapunov vectors [55,112]. The dynamical system (17) is simple enough to do this calculation analytically: this is done in the Methods. We find that the Lyapunov exponents are 0, $r - 3w^2$ and $2\beta_r R^2$ with corresponding covariant vectors at time $t = T$ (see Appendix A for a derivation and for the expression at arbitrary times)

$$\psi_1 = \begin{pmatrix} 0 \\ 1 \\ 0 \end{pmatrix} \quad \psi_2 = \frac{1}{N_2} \begin{pmatrix} 0 \\ -\gamma_i R\, h'(w) \\ 2r \end{pmatrix} \quad \psi_3 = \begin{pmatrix} 1 \\ 0 \\ 0 \end{pmatrix} \tag{20}$$

when $\alpha_r = 0$ and $\beta_i = 0$, and where N_2 is a normalization factor (the general case is similar, but the expressions are
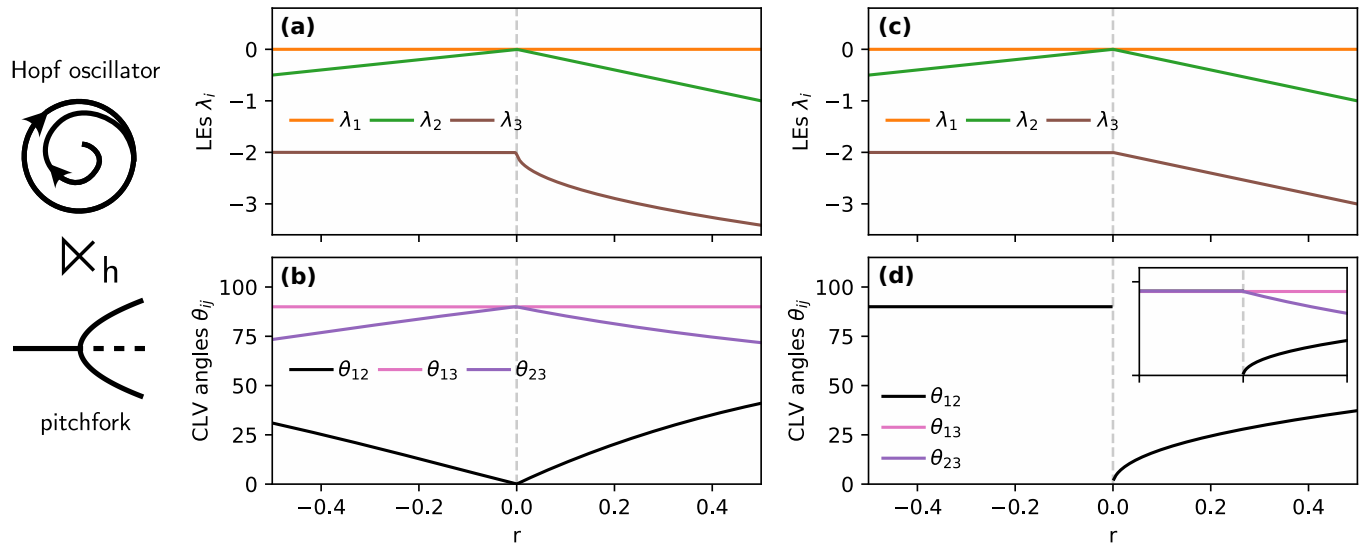
FIG. 3. Pitchfork of limit cycles. We consider a Hopf oscillator controlled by a pitchfork bifurcation through a coupling function h (represented by the symbol $\ltimes_h$) as in Eq. (17), leading to a pitchfork bifurcation of limit cycles. The Lyapunov exponents and the angles θ_{ij} between the covariant Lyapunov vectors are plotted as a function of the control parameter r, with two choices of the coupling function: (a, b) $h(w) = w$ and (c, d) $h(w) = w^2$. The angles θ_{ij} (b, d) is the angle between the CLVs c_i and c_j corresponding to λ_i and λ_j (a, c). The dashed gray line indicates the bifurcation point, where the Lyapunov exponents λ_1 and λ_2 both vanish and the corresponding CLVs align. In panel (b), the behavior of the CLVs is continuous through the bifucation. In panel (d), in contrast, the angle θ_{12} (black line) jumps from a finite value to zero when $r \to 0^-$. For clarity, we have plotted only θ_{12} in panel (d); the other angles are shown in the inset. We have set $\alpha = 1 + i$, $\beta = -1$, $\gamma = 1 + i$ in Eq. (17).

longer: see Appendix A). In these expressions, R and w are shorthands for their value on the current attractor as a function of the system parameters, and the vectors are written in the basis of perturbations $\delta X = (\delta x_1, \delta x_2, \delta w)$; see Appendix A for details.

Consider first the case in which $h(w) = w$, so $h'(w) = 1$ [Fig. 3(a) top]. At the bifurcation, $\psi_2 \to (0, 1, 0)$ when $r \to 0$, independent of whether the limit is taken from above or below. Near the bifurcation, we have essentially $\psi_2 \sim (0, 1, 2r)$, so the angle between ψ_1 and ψ_2 goes to zero: the two covariant Lyapunov vectors become parallel.

Consider now the case in which $h(w) = w^2/2$, so $h'(w) = w$ [Fig. 3(a) bottom]. When we approach the bifurcation from positive values $r \to 0^+$, the stable branches of solutions are $w = \pm\sqrt{r}$, so $\psi_2 \sim (0, \sqrt{r}, r) \to (0, 1, 0)$. As previously, the two vectors ψ_1 and ψ_2 become identical. However, when we approach the bifurcation from negative values ($r \to 0^-$), the stable branch is $w = 0$ and $\psi_2 \to (0, 0, 1)$, so the two covariant Lyapunov vectors do not become parallel in a continuous way. The coalescence of covariant Lyapunov vectors still occurs, but there is a discontinuity in the Lyapunov vectors at the bifurcation. As we shall see in Sec. V, this analytically tractable toy model exemplifies a situation that generically occurs in asymmetrically coupled oscillators.

D. Pitchfork of chaotic attractors

To conclude this section, we go beyond limit cycles and consider the symmetric coalescence of more complex attractors. As an example, we now discuss a pitchfork bifurcation of chaotic attractors. (We also refer to Appendix C for a

discussion on limit tori.) To do so, we take f in Eq. (16) to be a Lorenz attractor, which is a prototypical example of chaos [113,114]. Accordingly, we consider [115]

$$
\begin{aligned}
\dot{x} &= \sigma(y - x) + \gamma w, \\
\dot{y} &= x(\rho - z) - y + \gamma w, \\
\dot{z} &= xy - \beta z + \gamma w, \\
\dot{w} &= rw - w^3,
\end{aligned}
\tag{21}
$$

where we have chosen a linear coupling $g(\vec{x}, w) = \gamma w$. Due to the nonperiodicity of a chaotic attractor, there is no simple way to select a distinguished point where to compute the CLV for each choice of r, as we did for limit cycles. Instead, we compute the average $\langle|\theta_{ij}|\rangle$ over the attractor of the angles θ_{ij} between the CLVs c_i and c_j. As the CLVs are covariant with respect to the dynamics, they are parallel all along the attractor if they are parallel at one point. Figures 4(a) and 4(b) show that the CLVs become parallel at the bifurcation point $r = 0$ where the chaotic attractors merge. On one side of the bifurcation, a single chaotic attractor is present [Fig. 4(c)], while two of them coexist on the other side [Fig. 4(d)].

E. Generalization beyond pitchfork-like bifurcations

In this paper, we focus on pitchforks of attractors as described by Eq. (16). One can also consider a generalization of Eq. (16) in which the pitchfork bifurcation in Eq. (16b) is replaced with another bifurcation, such as a saddle-node or a transcritical bifurcation, in the same way as the so-called drift-transcritical bifurcation [97,98,119,120] can be obtained from the drift-pitchfork bifurcation (13). These are likely to
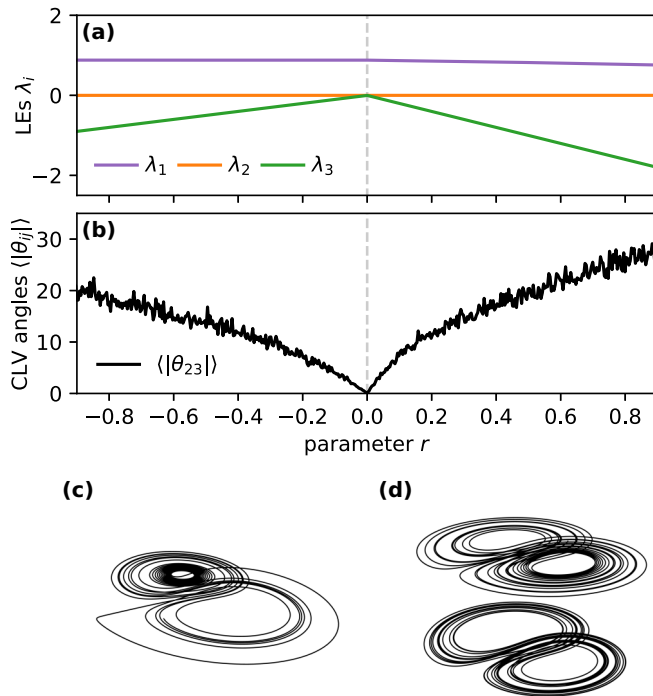
FIG. 4. Pitchfork of chaotic attractors. Following the general procedure of Eq. (16), we construct a pitchfork of chaotic attractors by controlling the Lorenz system [113,114] by a pitchfork. The full dynamical system is given in Eq. (21). The Lyapunov exponents are plotted with respect to the bifurcation parameter r in panel (a). The angle between the covariant Lyapunov vectors c_2 and c_3, averaged over the trajectory, is plotted in panel (b). On one side of the bifurcation (for $r < 0$), a single chaotic attractor is present (c). On the other side ($r > 0$), two chaotic attractors coexist (d), in addition to a chaotic repeller [not pictured in panel (d)]. At the bifurcation ($r = 0$), the Lyapunov exponents λ_2 and λ_3 [orange and green curves in panel (a)] vanish, while the angle between the corresponding CLVs also vanishes (b). We have set $\sigma = 10$, $\beta = 8/3$, $\rho = 28$, $\gamma = 5$ in Eq. (21). Equation (21) is numerically integrated using `DifferentialEquations.jl` [116]. The LEs and CLVs are computed using the algorithms of Refs. [47,51,117,118]. The average angles are computed by randomly choosing points along the chaotic attractor. We have set $r = -1$ (c) and $r = 100$ (d).

occur in situations where the $\mathbb{Z}_2$ symmetry associated with the pitchfork bifurcation is broken, making the bifurcation imperfect [21]. We refer to [34] and references therein for a discussion on bifurcations of limit cycles. This leads to other ways of merging/splitting attractors, that can also be accompanied with generalized exceptional points.

As an example, consider the dynamical system

$$\dot{\phi} = w \tag{22a}$$

$$\dot{w} = r - w^2 \tag{22b}$$

which is similar to Eq. (13), except that w is ruled by the normal form of a saddle-node bifurcation (rather than a pitchfork bifurcation). When ϕ is a phase variable, this equation describes the merging of a stable limit cycle with an unstable limit cycle at $r = 0$, leaving no attractor or repeller in phase space. As in Sec. III A, the bifurcation corresponds

to an exceptional point of the Jacobian. In less symmetric situations, this couldn't be captured by a time-independent effective Jacobian and we would need to resort to covariant Lyapunov vectors.

In addition, we note that the all the bifurcations we consider can arise in spatially extended systems, in which Eq. (16) (or variants) describes the dynamics on an invariant manifold. Simple examples can be obtained by adding a diagonal diffusive term to the normal form (16). Other examples include drifting defects and localized states [97,120–122], or nonreciprocal pattern formation [26].

IV. PHYSICAL CONSEQUENCES

In this section, we discuss the physical consequences of generalized exceptional points. First, we discuss how a system close to a generalized EP responds to small perturbations in Sec. IV A. The key point is that this response is not reciprocal (Sec. IV A). This occurs irrespective of the value of the Lyapunov exponent (finite or not) at the generalized exceptional point. When the corresponding Lyapunov exponent vanishes, this mechanism may lead to a pileup of perturbations along a certain direction in tangent space. This occurs because the nonreciprocity of the response is combined with the softening (critical slowing down) typical of criticality near a bifurcation [123]. In particular, this can lead to the destruction of isochrons, in which points in the basin of a limit cycle do not have a well-defined asymptotic phase (Sec. IV B). We also consider the effect of noise on a system near a generalized exceptional point (Sec. IV C). We find that the flatness of the response leads to an increased sensitivity to noise (Sec. IV C 1). In addition, on one side of the bifurcation, the presence of multiple attractors with different properties leads to the generation of telegraph noise from the white noise to which the full system is submitted (Sec. IV C 2).

A. Generalized EPs as atoms of nonreciprocity

The tangency of two CLVs $\vec{c}_1$ and $\vec{c}_2$ leads to a nonreciprocal coupling between perturbations about the corresponding directions. This arises irrespective of whether the corresponding Lyapunov exponents are finite or not. Far away from tangencies, when $\vec{c}_1$ and $\vec{c}_2$ are approximately orthogonal, a perturbation δX initially along $\vec{c}_1(0)$ essentially stays along $\vec{c}_1(t)$ (the same for $\vec{c}_2$). On the other hand, when $\vec{c}_1 \simeq \vec{c}_2$, a nonreciprocal response emerges. To illustrate this, let us consider a situation where a perturbation along the direction $\vec{c}_1^{\perp}$ orthogonal to the two approximately parallel CLVs $\vec{c}_1 \simeq \vec{c}_2$, as represented in Fig. 5. In such a case, it will eventually align with $\vec{c}_1$ [Fig. 5(a)]. The converse is not true: a perturbation along $\vec{c}_1$ stays along $\vec{c}_1$ [Fig. 5(b)]. In Figs. 5(c) and 5(d), we compare the fate of infinitesimal perturbations of a trajectory of Eq. (17) in the two cases of Fig. 3, corresponding to continuous and discontinuous behaviors of the CLVs. As expected, there is no mode interconversion in the discontinuous case, because the CLVs are orthogonal on this side of the bifurcation. This illustrates that the covariant Lyapunov vectors, not the Lyapunov exponents [124], are at the origin of the nonsymmetric mode interconversion.
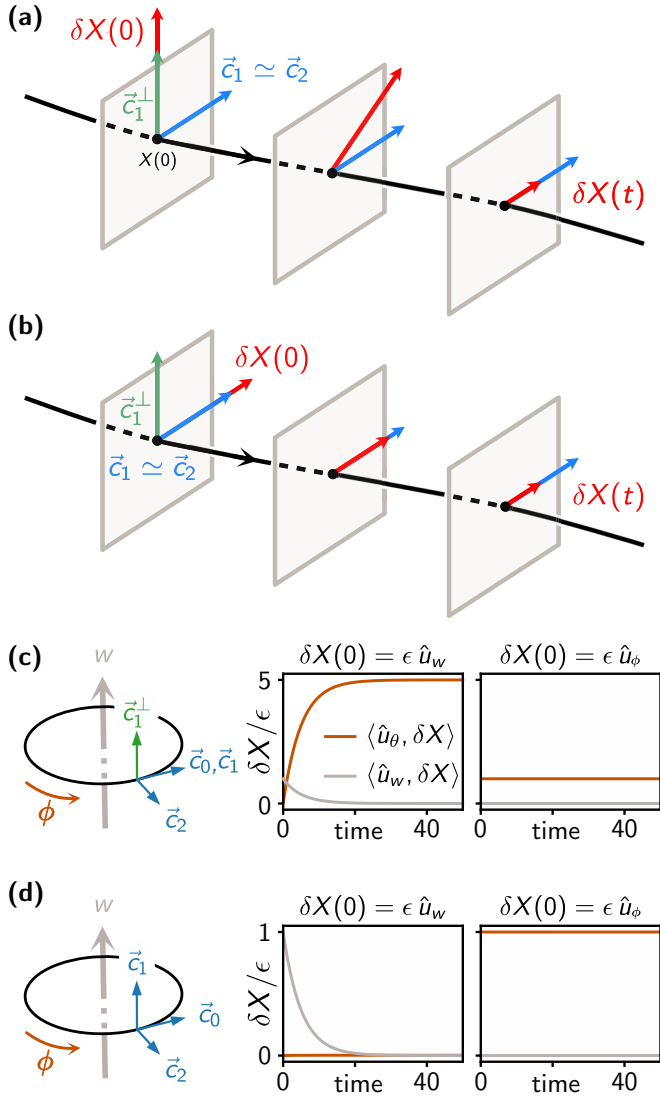
FIG. 5. Effect of a generalized exceptional point on perturbations. (a, b) When two CLVs $\vec{c}_1$ and $\vec{c}_2$ (in blue) are approximately parallel, there is a "missing" direction $\vec{c}_1^{\perp}$ (in green) in tangent space (light gray square), approximately orthogonal to $\vec{c}_1$ and $\vec{c}_2$ [125]. In panels (a) and (b), we sketch the evolution $\delta X(t)$ of a perturbation $\delta X(0)$ (in red) along the trajectory (black) in this situation. The relaxation of perturbations is nonreciprocal. In panel (a), the perturbation initially along $\vec{c}_1^{\perp}$ gradually aligns with $\vec{c}_1$. In panel (b), the perturbation initially along $\vec{c}_1$ stays along this direction. The evolution of the amplitude depends on the Lyapunov exponents. (c, d) The nonreciprocal relaxation described in panels (a)–(c) relies on the angles between CLVs. This allows us to distinguish between the continuous and discontinuous behaviors discussed in Sec. III C. We simulate Eq. (17) for (c) the continuous case $h(w) = w$ [like in Figs. 3(a) and 3(b)] and (d) the discontinuous case $h(w) = w^2$ on the discontinuous side of the bifurcation [like in Figs. 3(c) and 3(d)]. We compare a trajectory on the limit cycle to a perturbed trajectory: a perturbation $\Delta X(t = 0) \sim \epsilon$ along w is added as an initial condition, in the limit where $\epsilon \rightarrow 0$. The nonreciprocal relaxation does not occur when the CLVs are orthogonal (d). We have taken $r = -0.2$, $\alpha = 1 + i$, $\beta = -1$, $\gamma = 1 + i$, and $\epsilon = 0.001$.

B. EP-induced destruction of isochrons

Points starting in the basin of attraction of a limit cycle eventually end up on the limit cycle. One may ask what is the eventual dephasing between two such points. The answer to this question is provided by the notion of isochrons [126–134]. Under certain conditions, the notion of isochron can be extended to transient dynamics such as fixed points or excitable systems [132,133,135–137], heteroclinic orbits [138], or chaotic attractors [139–141]. The main idea is that the n-dimensional basin of attraction of the limit cycle can be decomposed into slices invariant under one period of evolution. These slices, called isochrons, essentially consist of all the points that eventually have a certain asymptotic phase. In more technical terms, isochrons provide a foliation of the basin of attraction by a one-parameter family of $(n − 1)$-dimensional hypersurfaces parameterized by the asymptotic phase $\phi \in S^1$ and that intersect the attractor transversally. Isochrons have been used to analyze the response and controllability of oscillators, including their transient dynamics, excitability, and synchronization [133,136,142]. They are also important tools to perform model reduction [126,143].

In this section, we show that the presence of a generalized exceptional point can lead to the destruction of isochrons. As we have seen in Sec. II C 1, the CLV $\vec{c}_* = \dot{X}$ with Lyapunov exponent $\lambda_* = 0$ associated with time-translation invariance is, by definition, tangent to the limit cycle. Away from (generalized) exceptional points, it can be shown that the hyperplane tangent to the isochron at position X forms the eigenspace spanned by the $n − 1$ CLVs (or Floquet eigenvectors) with finite Lyapunov exponents (see, for instance, Ref. [[126], Sec. 3.4]).

Figures 6(a)–6(c) schematically represents this behavior. As a CLV with finite exponent ($\vec{c}_2$ in the figure) tends to align with $\vec{c}_*$ (along the limit cycle, which is drawn in black), the isochrons (pink lines/hypersurfaces) become more and more tangent to the limit cycle. At an exceptional point, the isochrons are not well defined anymore. Equivalently, the asymptotic phase is not well defined [144]. Figures 6(d)–6(f) show isochrons computed using the method of Ref. [132] for the dynamical system defined by Eq. (17). As we approach the bifurcation at $r = 0$, the isochrons (colored lines) make an angle with the limit cycle (black line), which goes to zero at the bifurcation. This destruction of isochrons at generalized exceptional points has drastic consequences: even tiny perturbations lead to unbounded dephasings at long times [145].

C. Effect of noise

We now show that adding noise near a generalized exceptional point can produce striking effects: noise is amplified with an arbitrarily large factor, and colored noise is generated from white noise. On one side of the bifurcation, a random telegraph noise is generated as the system jumps between the two stable attractors heralded by the generalized EP. We illustrate these effects in the case of limit cycles.
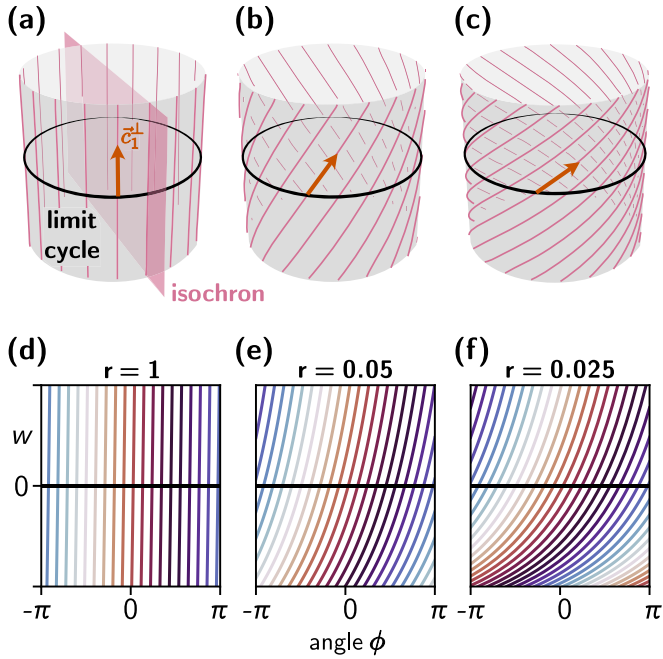
(a) **(b)** **(c)**

(d) **(e)** **(f)**

FIG. 6. Isochrons and Floquet vectors. In panels (a)–(c), we schematically show intersections of the isochrons with a cylinder (in purple) in the normal form Eq. (23) when approaching a generalized exceptional point (panels (a)–(c), corresponding to increasing closeness to the generalized EP). The limit cycle is drawn in black. The CLV (or Floquet eigenvector) $\vec{c}_2$ drawn in red, which has a finite Lyapunov, coalesces with the CLV $\vec{c}_* \equiv \vec{c}_1$ (in blue) with zero Lyapunov exponent that is tangent to the limit cycle (and corresponds to a dephasing). One entire isochron (a hypersurface of codimension one) is also represented as a purple plane in panel (a). In panels (d)–(f), we show slices of the isochrons of the dynamical system in Eq. (17) computed numerically. The limit cycle located at $w = \sqrt{r}$ is shown as a thick black line. As the generalized exceptional point at $r = 0$ is approached (from (d) to (f)), isochrons tilt towards the limit cycle. In the limit $r \to 0$, the isochrons are not transversal to the limit cycle anymore and cease to be well-defined. Colors label different isochrons, and the w axis ranges from $\sqrt{r} - 0.1$ to $\sqrt{r} + 0.1$. Isochrons are computed using the method of Ref. [132]. We have set $\alpha = 1 + i$, $\beta = -1$, $\gamma = i$, $h(w) = w$, and (d) $r = 1$, (e) $r = 0.05$, (f) $r = 0.025$.

To do so, we now consider a noisy version of the normal form in Eq. (13) [and Eqs. (17) and (18)]

$$\dot{w} = rw - w^3 + \eta_w(t), \tag{23a}$$

$$\dot{\phi} = \omega_0 + \omega_1 w + \eta_\phi(t), \tag{23b}$$

in which ω_0 and ω_1 are characteristic frequencies, and η_w and η_ϕ are Gaussian white noises satisfying $\langle \eta_i(t) \rangle = 0$ and $\langle \eta_i(t)\eta_j(t') \rangle = 2T_i \delta_{ij}\delta(t - t')$ (i, j label w, ϕ). We assume that $\omega_0 = 0$ (the $\omega_0 \neq 0$ can be reduced to this one by going in a comoving frame). When $\omega_1 = 0$, the two equations are decoupled. In this case, the random variable ϕ is the Wiener process corresponding to η_ϕ, so it has zero mean and its variance scales as t.

Now let us consider the case in which $\omega_1 \neq 0$. As the equation for w is fully decoupled from the ϕ equation, we can proceed in two steps. First, note that the variable w describes a Brownian particle in the potential $V(w) = -[rw^2/2 - w^4/4]$.

We consider separately the cases where $r < 0$ (Sec. IV C 1) and $r > 0$ (Sec. IV C 2).

1. Enhancement of noise by generalized EPs

We first consider the situation where $r \leqslant 0$. In this case, the potential has a single minimum at $w = 0$. In a nutshell, the noise on w is converted into noise in x with an arbitrarily large (or small) conversion ratio [for instance, proportional to ω_1 in Eq. (23)]. Approaching the generalized exceptional point ($r \to 0$), the potential landscape for w becomes flatter, affecting the properties of the noise. What are the consequences on fluctuations of the variable of interest ϕ? Neglecting the additional noise η_ϕ, a simple calculation (see Appendix F) shows that $\langle \phi \rangle^2 = 0$ and that in the limit where $|r| \to 0$, the variance of $\phi(t)$ at long times is

$$\langle \phi^2 \rangle \sim A\omega_1^2 t \tag{24}$$

in which $A \simeq 0.97499$ is a prefactor of order one. By analogy with particle diffusion, the slope D in the relation $\langle \phi^2 \rangle \sim Dt$ is called a phase diffusion coefficient [126]. We have seen that here $D = A\omega_1^2$. Notably, the effective phase diffusion coefficient does not depend on T_w. As a point of comparison, we find that $D = \omega_1^2(2T_w/r^2)$ when $r < 0$ is large enough to neglect the nonlinear term (in this limit, w is an Ornstein-Uhlenbeck process). Note that the phase diffusion coefficient can be arbitrarily large in both cases, due to the coefficient ω_1. As we show in Appendix F 3, it is even possible to find situations where the effective diffusion coefficient increases when noise strength is reduced. Similar results have been obtained in models of active matter, in which Eq. (23) can represent an active Brownian particle in a nonlinear potential [146–149]. The fact that the phase diffusion coefficient D is independent of the strength of the noise T_w may look paradoxical, as it suggests that a finite D would persist with no noise at all. The paradox is only apparent: the asymptotic diffusive regime only takes place after a transient with characteristic time $T_c \sim 1/\sqrt{T_w}$, which diverges as $T_w \to 0$ (see Appendix F) [150].

2. Integrated telegraphic noise from coalescing attractors

When $r > 0$, the potential V is a double well. When the noise is small enough, the particle spends a long period in each well, separated by quick jumps between the wells. This intermittent process is approximately described by the Ahrenius-Kramers-Eyring theory and can be approximated by a telegraph process [151]. In this approximation, $w(t) = \pm 1$ for random durations $\tau_\pm = \tau$ (the double well is symmetric) following an exponential distribution with probability density function (pdf)

$$p(\tau) = \frac{1}{\tau^*} e^{-\tau/\tau^*}, \tag{25}$$

where

$$\tau^* \equiv \mathbb{E}[\tau] = \frac{2\pi}{|V''(w^*)| V''(w_\pm)} e^{[V(w^*) - V(w_\pm)]/T} \tag{26}$$

is given by the Eyring–Kramers-Arrhenius formula in the limit where $T \to 0$ (see [152–156] and references therein), in which w^* is the position of the barrier (maximum of V) and
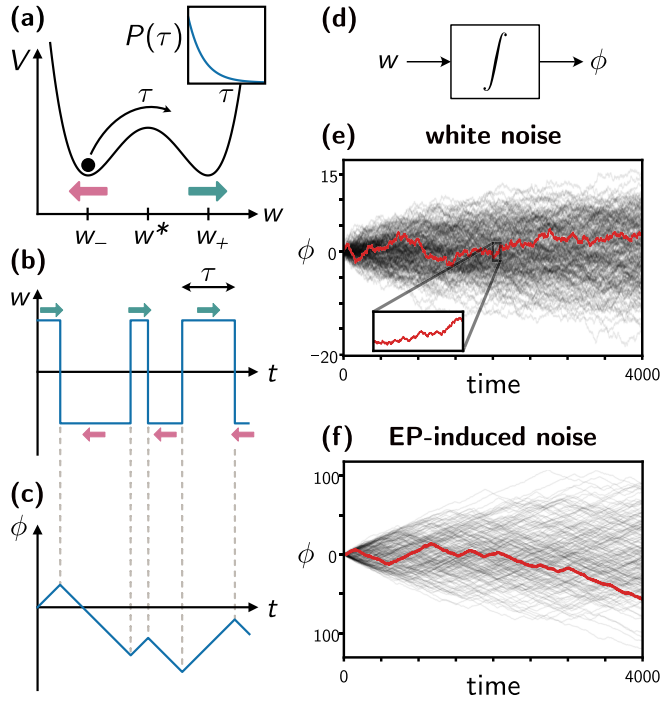
FIG. 7. Telegraph noise from coalescing attractors. Applying a weak noise produces stochastic jumps between attractors. This is illustrated in the simple case of Eq. (23). The two stable limit cycles are labeled by the minima $w_\pm$ of a double potential $U(w)$ (a). The sojourn times τ in each attractor are random variables, approximately following an exponential distribution (inset) described by the Ahrenius-Kramers-Eyring theory. As a consequence, w can be approximated as a random telegraph process (b). The state of the system then drifts along the attractor at a speed determined by $w(t)$. In (c), we have shown a schematic of the position ϕ on the attractor (e.g., the phase of the limit cycle) as a function of time, in the simple case where the angular velocity is directly proportional to w [see Eq. (23)]. Schematically, ϕ is obtained by integrating w (d). In panels (e) and (f) we compare the results of numerical integrations of Eqs. (23) for different realizations of the noise, with $\omega_1 = 0$ (d) and $\omega_1 \neq 0$ (e). An arbitrary trajectory has been highlighted in red. We have set $r = 0.22$, $\omega_0 = 0$, $\omega_1 = 0.1$, $T_w = T_\phi = 0.1$. We do not assume that ϕ is periodic.

$w_\pm$ is the position of the well (minimum of V); see Fig. 7(a). Here, with $V(w) = -rw^2/2 + w^4/4$, we find

$$\tau^* = \frac{\pi}{r^2} \, e^{r^2/4T}. \tag{27}$$

The telegraph noise generated by this process is a non-Gaussian, colored noise that tends to drive out of equilibrium the system on which it is applied [157–165]. On both sides of the bifurcation, the amplitude of the noise is proportional to the magnitude of the function g in Eq. (16) which can in principle be arbitrarily large or small.

The fate of ϕ can be understood by first ignoring the noise η_ϕ. In this case, $\dot\phi = \omega_1 w$. As a consequence, two effects occur. First, ϕ is composed of branches with positive and negative slopes $\omega_1 w_\pm$, obtained by integrating the random telegraph signal. The corresponding signal is highly correlated at short times, becoming diffusive only at long times. Second, the standard deviation of ϕ is proportional to ω_1, so it can

be orders of magnitude larger than the standard deviation of the white noise η_w acting on the variable w. Both effects can be directly observed in numerical simulations of the stochastic differential equation (23). In Fig. 7, we compare (i) in Fig. 7(e) the case where $\omega_1 \equiv 0$ (so there is only a Gaussian white noise) and (ii) in Fig. 7(f) the case where $\omega_1 \gg T_\phi$ and (so the telegraphic noise is large compared to the pre-existing Gaussian noise). In case (i), ϕ is directly a Wiener process (i.e., a Brownian motion). Therefore, it is scale invariant and diffusive (as $\langle\phi^2\rangle \propto t$). Note $\langle\phi\rangle = 0$. In the case (ii), $\phi(t)$ is a succession of upward and downward slopes with values $\pm w_c = w_\pm = \pm\sqrt{r}$, extending over durations distributed exponentially, following Eq. (25).

When the measurement time scales are small compared to the characteristic time τ^* of reversals, this succession of upward and downward slopes can be directly observed. This is, for instance, the case in a recent experiment where a plate freely rotates in a Rayleigh-Bénard convection cell [30] (Appendix G). When the measurement timescale is large compared to τ^*, the process we described has indirect consequences. This is what happens in the case of coupled lasers, in which the consequence is a two-color laser characterized by a power spectrum with two peaks (corresponding to the two frequencies of oscillation of the two limit cycles), as it has been experimentally observed in Ref. [86] (see also Refs. [87,88] and SI Sec. XII of Ref. [26]).

V. EXAMPLES

In the following sections, we provide more realistic examples of systems with bifurcations associated with generalized exceptional points gathered from different fields. Each situation follow a similar scenario as in Fig. 3. Figures 8–11 show that in each system, a bifurcation separates a region with a single stable attractor and a region with two stable attractors and an unstable one. The numerical computation of the Lyapunov exponent and covariant vectors demonstrate that two Lyapunov exponents become degenerate at the bifurcation, where the corresponding vectors align at least on one side.

A. Coupled nonlinear oscillators

We first show that coupling two nonlinear oscillators in a nonreciprocal way typically leads to a pitchfork bifurcation of limit cycles. To do so, we consider the dynamical system

$$\begin{bmatrix} \dot z_1 \\ \dot z_2 \end{bmatrix} = \begin{bmatrix} (a + i\omega) + b|z_1|^2 & a_{12} \\ a_{21} & (a + i\omega) + b|z_2|^2 \end{bmatrix} \begin{bmatrix} z_1 \\ z_2 \end{bmatrix} \tag{28}$$

consisting of two copies of the normal form of a Hopf bifurcation (Hopf oscillators) for the complex variables z_n coupled by the terms a_{12} and a_{21}. Depending on the value of $a_+ = [a_{12} + a_{21}]/2$ and $a_- = [a_{12} - a_{21}]/2$, the Hopf oscillators can be in an aligned, antialigned, or chiral state. When the coupling of the oscillators is sufficiently nonreciprocal, the aligned/antialigned state transitions to the chiral state, and a bifurcation occurs such that the steady state of the dynamical system will have a finite angle between the oscillators, which approaches 90° as a_- becomes large. There are two such steady states, one where z_1 chases z_2 as the system
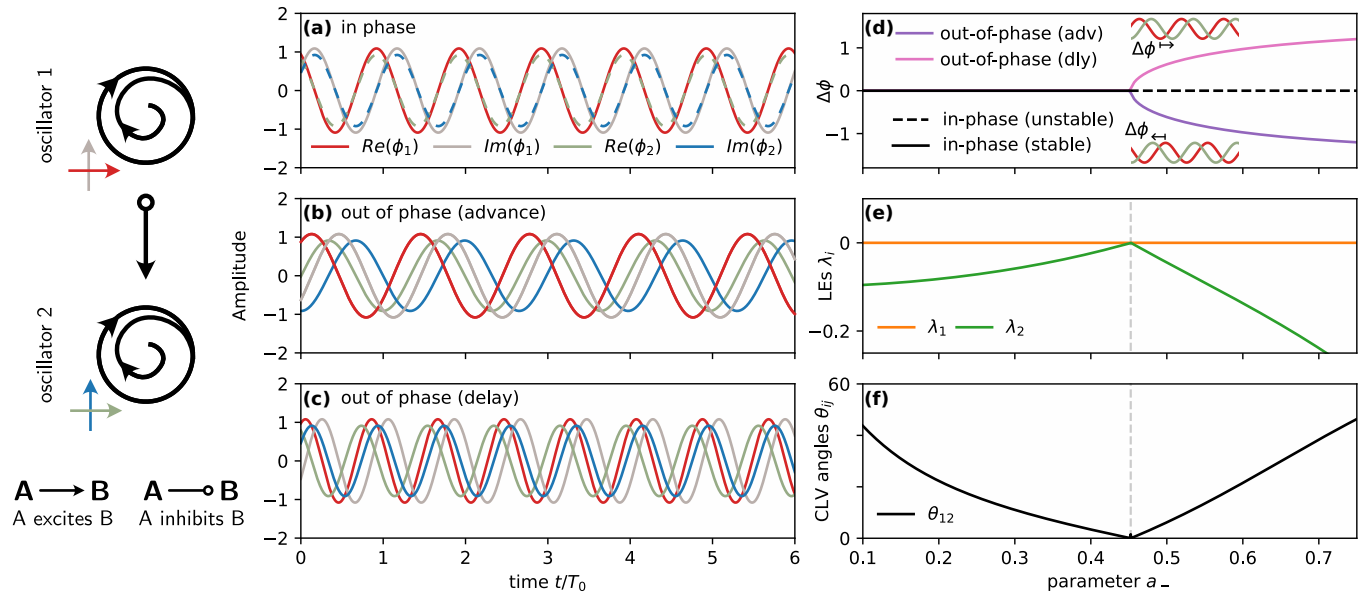
FIG. 8. Coupled nonlinear oscillators. We simulate the coupled nonlinear oscillators given in Eq. (28). Depending on the value of the parameter a_-, we observe different behavior illustrated by the time series in panels (a)–(c). When $a_- < a_-^c \approx 0.22625$, the two oscillators exhibit synchronized oscillations corresponding to a single limit cycle (a). When $a_- > a_-^c$, the two oscillators become out of phase (b), (c). Depending on the initial condition, the phase difference $\Delta\phi$ between the oscillators $z_1(t)$ and $z_2(t)$ can either be positive (c) or negative (d). Hence, there are two stable limit cycles. The phase difference is plotted as a function of a_- in panel (d). At the bifurcation point $a_- = a_-^c$, a generalized exceptional point occurs, as shown in panels (e) and (f). In panel (e), the largest Lyapunov exponents λ_1 and λ_2 are plotted. We always have $\lambda_1 = 0$ because the dynamical system is autonomous. At the bifurcation point $a_- = a_-^c$, the second Lyapunov exponent λ_2 also vanishes. At the same time, the angle θ_{12} between the CLVs c_1 and c_2 vanishes (f), showing that a generalized exceptional point occurs. The CLVs are continuous across the bifurcation. We have set $a = \omega = -b = 1$, $a_+ = 0.05$. In panel (a), a_- is varied from 0.05 to 0.375. In panel (a), $a_- = 0.3$. In panels (b) and (c), $a_- = 0$.

oscillates, and one where z_2 chases z_1. The symmetry of the system is spontaneously broken, determining which Hopf oscillator leads and which follows. The transition from the aligned to chiral state occurs at an exceptional point, where one Lyapunov exponent becomes zero at the bifurcation, and the corresponding Lyapunov vectors become parallel at all points on the limit cycle, as shown in Fig. 2. The behavior of the model (28) is phenomenologically similar to the pitchfork of limit cycles with $h(w) = w$ analyzed in the previous section [compare Figs. 3(a) and 3(b) with Figs. 8(e) and 8(f)].

Writing $z_n = r_n e^{i\phi_n}$ in polar form, performing an adiabatic elimination of r_n (see, e.g., Ref. [166]) assuming $a_\pm \ll a$, we end up with

$$\partial_t \Delta\phi = 2(a_+ - a_-^2/a \cos\Delta\phi)\sin\Delta\phi, \quad (29a)$$

$$\partial_t \phi = \omega + a_- \sin\Delta\phi \quad (29b)$$

in which $\Delta\phi \equiv \phi_2 - \phi_1$ and $\phi = [\phi_1 + \phi_2]/2$. A series expansion for small $\Delta\phi$ and a rescaling leads to the normal form (19). Crucially, this allows us to identify the control variable w in the normal form Eq. (19) to the dephasing $\Delta\phi$ between the oscillators (namely, $w \propto \Delta\phi$). The two symmetric nonzero solutions $\Delta\phi_\pm$ of $\partial_t \Delta\phi = 0$ correspond to the two limit cycles that emerge at the bifurcation. This is a generic feature, which we will find in other examples of coupled oscillators (Secs. V B and V C).

B. Wilson-Cowan neurons

We next consider a simplified model of neural network dynamics, the Wilson-Cowan model [167,168]. The model describes the dynamics of the average firing rates x_i of coupled neurons, which evolve according to

$$\dot{x}_i = -x_i + \tanh\left(\sum_j A_{ij} x_j + h_i\right), \quad (30)$$

where the indices $i, j = 1, \ldots, N$ label neurons, h_i is an external forcing, and A_{ij} contains the couplings between the neurons. It is assumed that each neuron j is either excitatory, in which case it increases the firing rates of the neurons it influences ($A_{ij} \geqslant 0$ for all i) or inhibitory, in which case it decreases it ($A_{ij} \leqslant 0$ for all i). The coupling between an excitatory neuron and an inhibitory neuron is therefore nonreciprocal: more precisely, A_{ij} and A_{ji} have opposite signs. Here we consider the case of one excitatory plus two inhibitory Wilson-Cowan neurons and choose to use the coupling $A_{11} = \zeta$ as the bifurcation parameter. Here the angle between CLVs generally depends on the position on the limit cycle, because it is not a circle, except if the angle is zero (i.e., if two CLVs are parallel). To obtain comparable quantities for different values of the parameters, we arbitrarily select a particular point on the cycle (the one that maximizes one of the coordinates) for each value of ζ. The three limit cycles coalesce at a critical
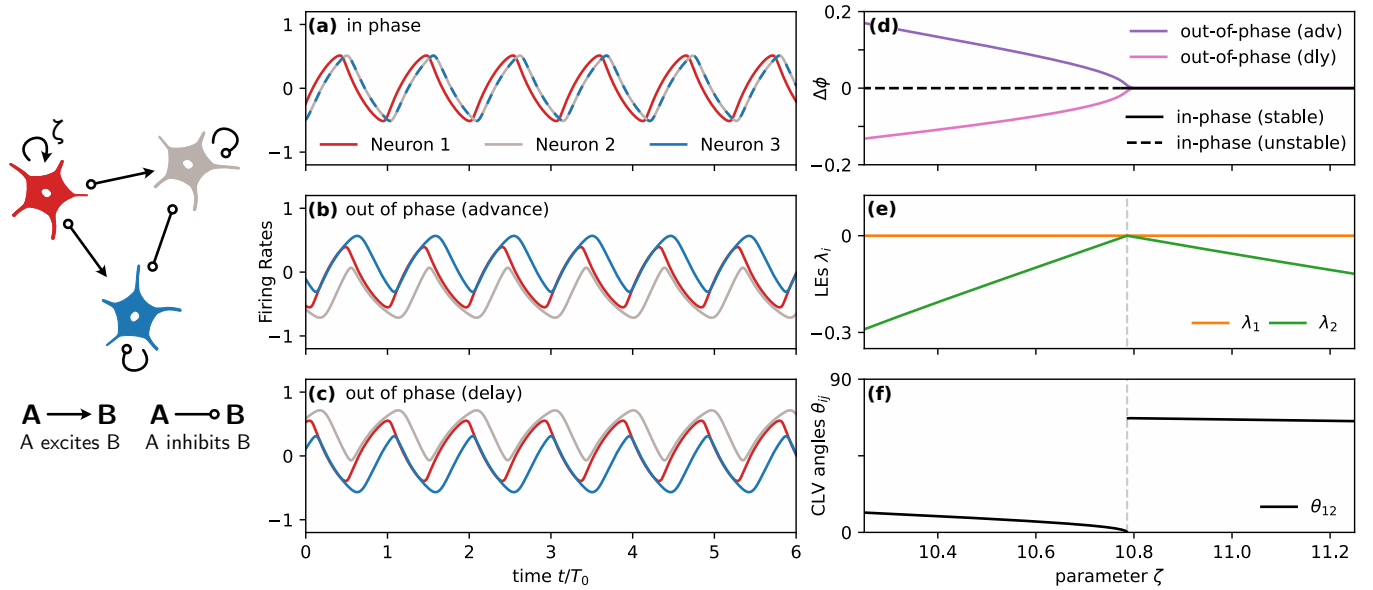
FIG. 9. Wilson-Cowan model. Panels (a)–(c) show time series of the Wilson-Cowan model in Eq. (30) for one excitatory neuron ($i = 1$) coupled to two inhibitory neurons ($i = 2, 3$). When $\zeta > \zeta_c \approx 10.786$, the firing rates of the two inhibitory neurons are in-phase oscillations corresponding to a limit cycle (a). When $\zeta < \zeta_c$, the two inhibitory neurons become out of phase (b), (c), and the phase difference $\Delta\phi$ depends on the initial condition, as there are two stable limit cycles. The phase difference is plotted as a function of ζ in panel (d). The two limit cycles correspond to phase advance (adv, purple) or delay (dly, pink). In panel (e), the largest Lyapunov exponents λ_1 and λ_2 are plotted ($\lambda_1 \equiv 0$ because the dynamical system is autonomous). At the bifurcation $\zeta = \zeta_c$, the second Lyapunov exponent λ_2 and the angle θ_{12} between the CLVs c_1 and c_2 vanish (f). This is a generalized exceptional point. The angle θ_{12} is discontinuous through the transition: it stays constant when $\zeta \to \zeta_c$ from the right. We have set $A_{11} = \zeta$, $A_{21} = A_{31} = 8$ in which $\zeta \geqslant 0$ can vary (for the excitatory neuron $j = 1$), $A_{12} = -4.5$, $A_{22} = 0$, $A_{32} = -4$, and $A_{13} = -7.5$, $A_{23} = -4$, $A_{33} = 0$ (for the inhibitory neurons $j = 2, 3$) and $h_i = 0$ for all neurons. In panel (a), $\zeta = 11$. In panels (b) and (c), $\zeta = 9$. Times are normalized by the period T_0 at ζ_c.

value ζ_c where a bifurcation occurs. The bifurcation is marked in Fig. 9 by a dotted line, where two Lyapunov exponents combine, while the angle between the corresponding CLVs goes to zero. The behavior of the Wilson-Cowan model (30) is phenomenologically similar to the pitchfork of limit cycles with $h(w) = w^2$ analyzed in the previous section [compare Figs. 3(c) and 3(d) with Figs. 9(e) and 9(f)]. This suggests that a slow manifold reduction of Eq. (30) would produce Eq. (17) near the bifurcation.

The merging and splitting of limit cycles has been suggested as a toy model of perceptual bistability for temporally periodic stimuli [168–170]. A simple example consists in a sequence of tones A and B with different frequencies repeated in ABA … patterns: the same sound can be heard as two separate sequences A-A-A- … and B-B-B- … with different periods, or as a single ABA-ABA- … sequence, and one can switch from one perception to the other and back. You can hear a demonstration in Ref. [171]. There is only one signal, but our brains can interpret it in different ways. These two different perceptions are distinguished by whether the tones are perceived to be synchronized or not. This information can be encoded in the in-phase and out-of-phase states of two coupled oscillators, which could therefore provide a mechanism for perceptual bistability [168]. In this context, the coalescence of two attractors corresponds to the confusion

between two percepts, that become indistinguishable at the bifurcation.

C. Rosenzweig-MacArthur prey-predator model

The notion of nonreciprocity is perhaps nowhere as striking as in ecology: predators eat prey, but prey rarely eat predators. Based on the results of Sec. V A, we expect that a nonreciprocal coupling may affect the phase coordination of the species. This phase coordination is believed to influence biodiversity in prey-predator and other consumer-resource models [172–175]. Essentially, the idea is that in-phase synchronization of, say, two predators opens a periodic opportunity for a third one to enter the system. However, the invading species may modify the phase coordination of the two original species, potentially breaking the conditions for invasion [172]. This motivates a precise analysis of the phase coordination before any invasion.

Here we consider two coupled versions of a minimal but realistic predator-prey model called the Rosenzweig-MacArthur model [20,176–178]. In our toy model, two kinds of prey and two kinds of predators are present. The prey are kind and hence they collaborate with each other and increase their respective populations in a mutualistic way. In contrast, the predators are unkind, so they compete and kill each other. This is summarized by the graph on the left side of Fig. 10. This
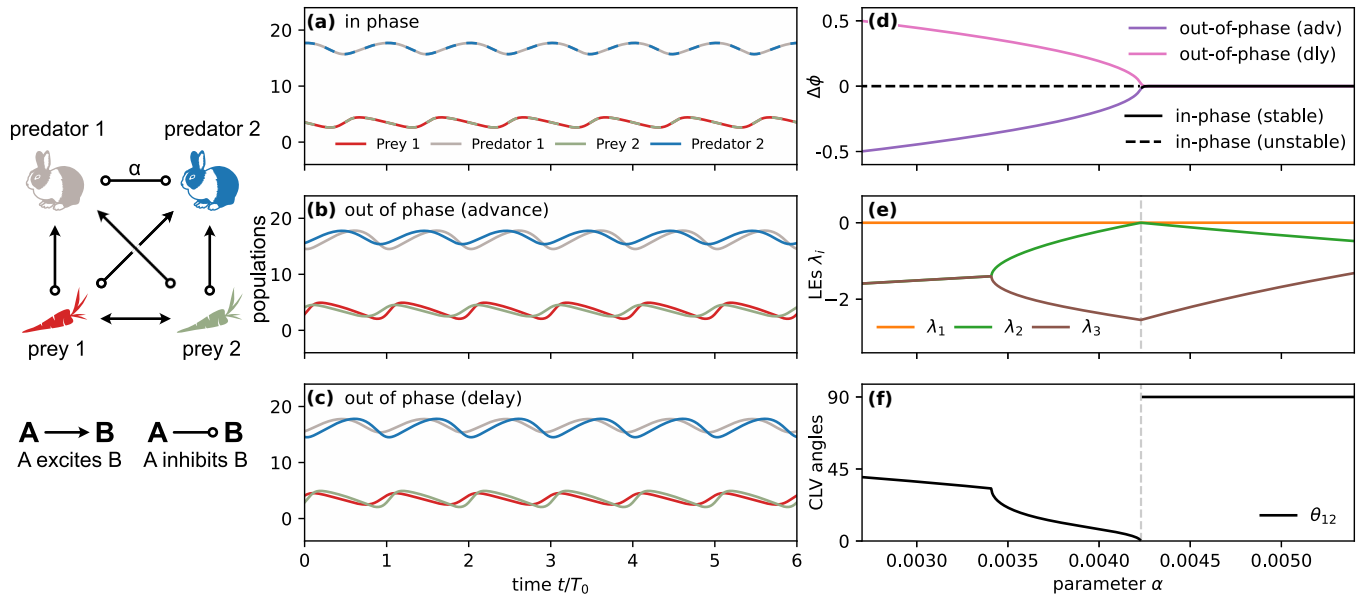
FIG. 10. Rosenzweig-MacArthur prey-predator model. We simulate the Rosenzweig-MacArthur model in Eq. (31), with two prey and two predators. The size of the populations of prey and predators evolve periodically in time (a)–(c). When $\alpha > \alpha_c \approx 0.00423$, the prey are in phase with each other, and the predators in phase with each other (a). When $\alpha < \alpha_c$, there is a dephasing $\Delta\phi$ between the two prey (and the two predators), positive or negative depending on the initial condition: two stable attractors are present. Panel (d) shows the phase difference between the two prey as a function of α (black line for the in-phase state of panel (a); purple and pink lines for the out-of-phase states of panels (b) and (c), respectively phase advance (adv) or delay (dly). At $\alpha = \alpha_c$ (gray dashed lines), a generalized exceptional point occurs. At the bifurcation, both the Lyapunov exponent λ_2 (e) and the angle θ_{12} between the CLVs c_1 and c_2 (f) vanish. The angle θ_{12} is discontinuous at α_c. We have set $s = 12$, $r = 12$, $k = 15.6$, $u_0 = 8$, $\epsilon = 0.1$, and α is varied from 0.0027 to 0.0054. In panels (a)–(c) the initial conditions are $\vec{x}(0) = (u_1(0), v_1(0), u_2(0), v_2(0)) = 2.8, 16.2, 4.9, 14.7$, and $\vec{x}(0) = 4.9, 14.7, 2.8, 16$. In panel (a), $\alpha = 0.0054$. In panels (b) and (c), $\alpha = 0.0024$.

model is described by the coupled differential equations

$$
\begin{aligned}
\dot{u}_1 &= r(u_0 - u_1)u_1 - k\frac{u_1 v_1}{1 + u_1} + \epsilon r(u_0 - u_2)u_2, \\
\dot{v}_1 &= k\frac{u_1 v_1}{1 + u_1} - sv_1 - \alpha v_2 v_1, \\
\dot{u}_2 &= r(u_0 - u_2)u_2 - k\frac{u_2 v_2}{1 + u_2} + \epsilon r(u_0 - u_1)u_1, \\
\dot{v}_2 &= k\frac{u_2 v_2}{1 + u_2} - sv_2 - \alpha v_1 v_2,
\end{aligned}
\tag{31}
$$

where u_1 and u_2 are the numbers (or concentrations) of prey, while v_1 and v_2 are the numbers of predators. The coefficient r measures the natural growth of prey (u_0 sets the capacity of the environment), s measures the natural decline of predators, and k measures predation, which reduces the number of prey while increasing the number of predators. Finally, ϵ measures the collaboration between prey and α measures the direct competition between predators. Again, we observe that the Lyapunov vectors become parallel at the bifurcation. The behavior of the Rosenzweig-MacArthur model (31) is phenomenologically similar to the pitchfork of limit cycles with $h(w) = w^2$ analyzed in the previous section [compare Figs. 3(c) and 3(d) with Figs. 10(e) and 10(f)].

Before the bifurcation [right side in Figs. 10(d)–10(f)], the two species of prey are synchronized together (and the two kinds of predators are synchronized together). After the bifurcation [left side in Figs. 10(d)–10(f)], this is not the case, and the two different limit cycles correspond to different

sequences of the local maxima of the different populations (e.g., u_1, u_2, v_1, v_2 versus u_2, u_1, v_2, v_1). Again, the splitting of the limit cycle leads to a finite phase delay between the two populations, that are neither in phase nor in antiphase. In the steady state, the dephasing takes two possible values corresponding to the two stable limit cycles, depending on which populations is in advance.

While our model is a simplified version of what could take place in realistic situations, we expect this phenomenon to occur in nature. For instance, nontrivial phase delays (neither zero nor π) have been observed in a laboratory experiment probing the food web structure of a plankton community isolated from the Baltic Sea [29,175]. In this case, the preys are phytoplankton species (picocyanobacteria and nanoflagellates), while the predators are zooplankton (rotifers and calanoid copepods). In Ref. [175], this situation is modeled using coupled Rosenzweig-MacArthur-like equations with more realistic couplings [175,179,180]. Figure 11 summarizes the model (see Appendix F4 for the equations) containing two preys species and two predator species (with a different interaction network compared to the model of Fig. 10). We now show that this model also exhibits a generalized exceptional point marking the bifurcation between a single limit cycle with populations in antiphase, and two stable limit cycles with a nontrivial phase delay. Figures 11(a)–11(h) show numerical simulations of the model before the bifurcation where there is a single stable limit cycle [Figs. 11(a)–11(c)] and after the bifurcation, where there are two stable limit cycles [Figs. 11(d)–11(f) and 11(g)–11(i)]. These are distinguished by a
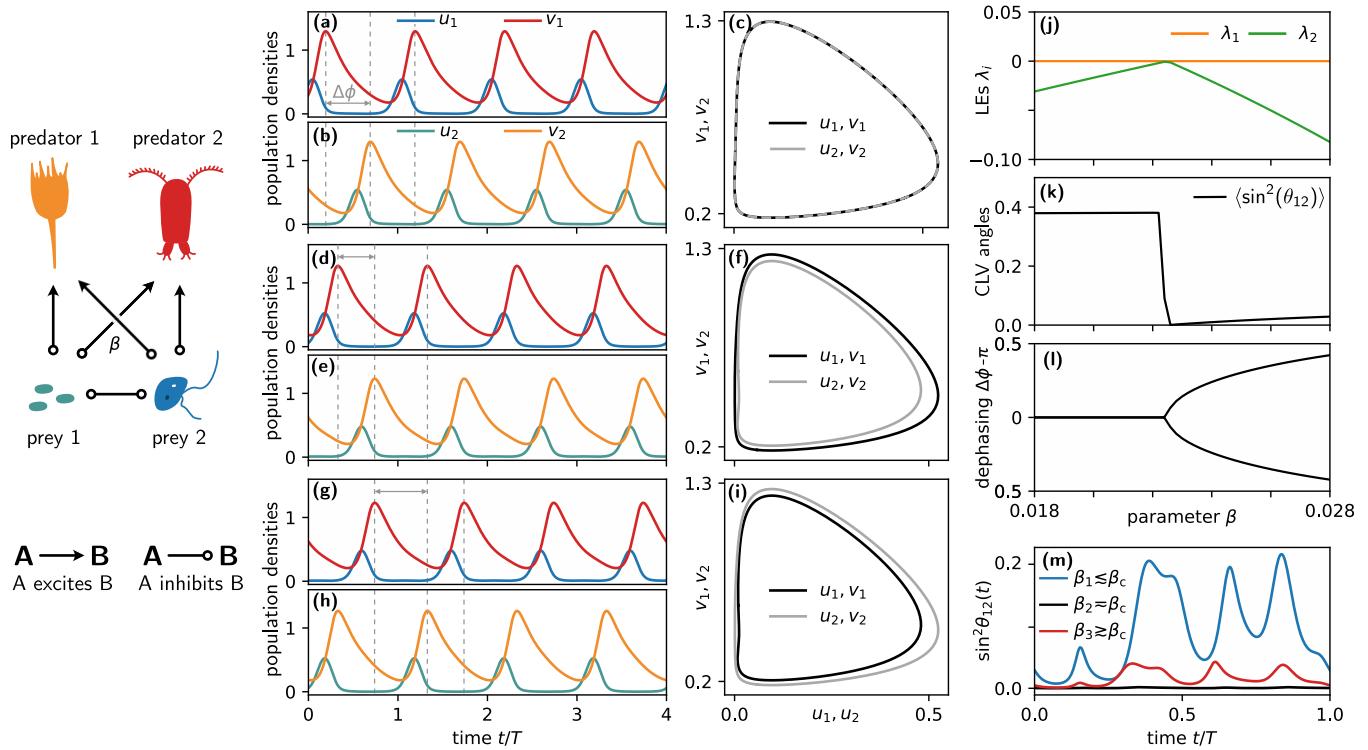
FIG. 11. Model of plankton food web. We simulate a set of coupled Rosenzweig-MacArthur-like equations given by Eq. (F27) and used in Ref. [175] to model laboratory experiments on a plankton food web isolated from the Baltic Sea [29]. This model describes the population densities of prey $u_i(t)$ and of predators $v_k(t)$, and involves a parameter β that quantifies the coupling through predation of the two coupled prey-predator systems. Below a critical value $\beta_c \simeq 0.02275$, a single limit cycle exists (a)–(c). Two stable limit cycles exist above the critical value, as shown in panels (d)–(f) and (g)–(i), respectively. At the bifurcation, both the Lyapunov exponent λ_2 (j) and the angle θ_{12} between the CLVs c_1 and c_2 (k) vanish. The angle θ_{12} is discontinuous from the left at β_c. Parameter values and initial conditions are given in Appendix F 4, after Eq. (F27).

dephasing $\Delta\phi$ between the species [in gray in Figs. 11(a), 11(b), 11(d), 11(e), 11(g), and 11(h)] that exhibits a pitchfork shape as the bifurcation parameter β is changed [Fig. 11(i)]. At the same time, the two largest Lyapunov exponents become degenerate [Fig. 11(j)] and the angle between covariant Lyapunov vectors vanishes [continuously from one side, discontinuously from the other; see Fig. 11(k)]. Our analysis of the model of Ref. [175] suggests the existence of two different limit cycles. The nontrivial dephasings observed in the experiment is indirect evidence supporting this statement. In principle, it could be directly verified experimentally. We note that it would have consequences on the correlations between species' abundances. In particular, two different results could be obtained for the same values of the couplings. In Sec. IV we show that the proximity to a generalized exceptional point typically leads to an increased effect of noise: it is therefore intriguing to ask what would be the consequences of stochastic fluctuations [181] on the ecological model.

VI. CONCLUSION AND PERSPECTIVES

In this article, we have shown that the tangency of covariant Lyapunov vectors provides a generalization of exceptional points to arbitrary nonlinear systems. Such an exact tangency occurs for the covariant Lyapunov vectors associated with vanishing Lyapunov exponents in a class of bifurcations describing the splitting and merging of extended invariant sets,

creating a Jordan blocks in their Lyapunov-Oseledets cocycle. This suggests intriguing parallels between classical dynamical systems [66,67] and quantum many-body systems [182]. In the case of limit cycles, we have shown generalized exceptional points can occur both continuously and discontinuously, depending on time-dependent symmetries of the cycles. By analyzing the effect of noise and perturbations in systems with generalized exceptional points, we find these systems exhibit an enhanced sensitivity to noise to small perturbations in addition to displaying a nonreciprocal response. For instance, in the case of limit cycles, isochrons become tangent to the limit cycle and are ill-defined at the bifurcation, and the effective diffusion coefficient on the attractor exhibits anomalous temperature dependence.

DATA AVAILABILITY

No experimental or measurement data were generated in this work. Numerical results can be regenerated with the open-source code archived at Zenodo [183].

APPENDIX A: COMPUTATION OF THE LYAPUNOV EXPONENTS AND VECTORS USING FLOQUET THEORY

In this appendix, we compute analytically the Lyapunov exponents and covariant Lyapunov vectors (also known as Floquet vectors) for the very simple system (17) using Floquet theory [184–186]. To do that, we harness the rotational symmetry of the system to evaluate the evolution operator in Eq. (7) directly by diagonalizing the Jacobian in a rotating frame.

1. Floquet theory

In this section, we recall basics of Floquet theory [184–186]. In the main text, we have introduced the evolution operator $U(t, t_0)$ in Eq. (7), defined as the unique solution of the Cauchy problem Eq. (6) with $U(t_0, t_0) = \text{Id}$, where Id is the identity matrix. In the case of periodic orbits, one can show that

$$U(t + T, t_0 + T) = U(t, t_0). \tag{A1}$$

In order to keep notations simple, we now set the origin of times so that $t_0 = 0$ and write $U(t) = U(t, t_0 = 0)$. As a consequence of the property $U(t + T, t_0 + T) = U(t, t_0)$, we have

$$U(t + nT) = U(t)[U(T)]^n \tag{A2}$$

for integer n. This suggests that the long-time evolution of the system is mainly controlled by the matrix $U(T)$, called the Floquet operator or monodromy matrix. This can be made precise by writing

$$U(t) = V(t)e^{tF} \tag{A3}$$

in which $F = (1/T) \log U(T)$ and $V(t) = U(t)e^{-tF}$ satisfies $V(t + T) = V(t)$. This decomposes the evolution operator in a periodic part $V(t) = V(t + T)$ and a nonperiodic part related to $U(T)$. The eigenvalues μ_i of $U(T)$ are called Floquet multipliers, and we also defined the Floquet exponents s_i such that $\mu_i = e^{s_i}$ (the exponents are related to the eigenvalues of F by a factor T).

In the case of a periodic orbit, the Lyapunov exponents λ_i are given by $\lambda_i = \log |\mu_i| = \text{Re}(s_i)$, while the covariant Lyapunov vectors are directly the eigenvectors of $U(T)$ (in case of degeneracies, the Floquet eigenvectors at least span the same spaces as the covariant Lyapunov vectors) [55,112].

2. Floquet analysis of the Hopf-pitchfork system

We start from Eq. (17) and compute the Jacobian (2). The variables are $X_1 = \text{Re}(z) \equiv x$, $X_2 = \text{Im}(z) \equiv y$, and $X_3 = w$. Matrices and vectors follow the ordering (X_1, X_2, X_3). Perturbations δX satisfy

$$\delta \dot{X} = J(X(t))\delta X. \tag{A4}$$

A direct computation shows that the Jacobian is

$$J(X) = \begin{pmatrix} \alpha'_r + \beta_r(3x^2 + y^2) - \beta_i 2xy & -\alpha'_i + \beta_r 2xy - \beta_i(x^2 + 3y^2) & [\gamma_r x - \gamma_i y]h' \\ \alpha'_i + \beta_i(3x^2 + y^2) + \beta_r 2xy & \alpha'_r + \beta_i 2xy + \beta_r(x^2 + 3y^3) & [\gamma_i x + \gamma_r y]h' \\ 0 & 0 & r - 3w^2 \end{pmatrix} \tag{A5}$$

in which $h' = dh/dw$.

Evaluating the Jacobian on the limit cycle solutions with radius R and angular frequency Ω (the expression of which is given as a function of the parameters in the main text), we find

$$J(t) = J(X(t)) = \begin{pmatrix} 2R^2[\beta_r c^2 - \beta_i cs] & -\Omega + 2R^2[-\beta_i s^2 + \beta_r cs] & R(\gamma_r c - \gamma_i s)h' \\ \Omega + 2R^2[\beta_i c^2 + \beta_r cs] & 2R^2[\beta_r s^2 + \beta_i cs] & R(\gamma_i c + \gamma_r s)h' \\ 0 & 0 & r - 3w^2 \end{pmatrix}, \tag{A6}$$

where we have temporarily set $c = \cos(\Omega t)$ and $s = \sin(\Omega t)$, and in which R and Ω are functions of the parameters of the system.

We then perform a time-dependent unitary change of basis

$$X \rightarrow X' = V(t)X \tag{A7}$$

with

$$V = \begin{pmatrix} \cos(\Omega t) & \sin(\Omega t) & 0 \\ -\sin(\Omega t) & \cos(\Omega t) & 0 \\ 0 & 0 & 1 \end{pmatrix} \tag{A8}$$

to go to the frame rotating at the frequency Ω about the w axis. In the rotating frame, perturbations $\delta X' = V(t)\delta X$ follow

$$\delta \dot{X}' = \dot{V}\delta X + V\delta\dot{X} = (\dot{V}V^{-1} + VJV^{-1})\delta X' \tag{A9}$$

so the Jacobian transforms as

$$J(t) \rightarrow J'(t) = \dot{V}V^{-1} + VJV^{-1}. \tag{A10}$$

Here this expression reduces to

$$J' = \begin{pmatrix} 2R^2\beta_{\mathrm{r}} & 0 & R\gamma_{\mathrm{r}}h' \\ 2R^2\beta_{\mathrm{i}} & 0 & R\gamma_{\mathrm{i}}h' \\ 0 & 0 & r - 3w^2 \end{pmatrix}. \tag{A11}$$

As J' does not depend on time, the solution of Eq. (A9) is

$$\delta X'(t) = \mathrm{e}^{tJ'}\delta X'(0). \tag{A12}$$

Hence, going back to the original reference frame,

$$\delta X(t) = U(t)\delta X(0) \tag{A13}$$

in which

$$U(t) = V^{-1}(t)\mathrm{e}^{tJ'}V(t). \tag{A14}$$

As $V(T) = 1$, we find that the Floquet operator is $U(T) = \mathrm{e}^{TJ'}$. Hence, the eigenvectors of $U(T)$ are identical to those of J', and the eigenvalues μ_i of $U(T)$ (Floquet multipliers) are obtained from the eigenvalues ϵ_i of J' as $\mu_i = \mathrm{e}^{T\epsilon_i}$. A direct calculation gives

$$\psi_1 = \begin{pmatrix} 0 \\ 1 \\ 0 \end{pmatrix},$$

$$\psi_2 = \frac{1}{N_2}\begin{pmatrix} h'R\gamma_{\mathrm{r}}(r - 3w^2) \\ h'R\big(\gamma_{\mathrm{i}}r + 2R^2(\beta_{\mathrm{i}}\gamma_{\mathrm{r}} - \beta_{\mathrm{r}}\gamma_{\mathrm{i}}) - 3\gamma_{\mathrm{i}}w^2\big) \\ (r - 2\beta_{\mathrm{r}}R^2 - 3w^2)(r - 3w^2) \end{pmatrix},$$

$$\psi_3 = \frac{1}{\sqrt{\beta_{\mathrm{r}}^2 + \beta_{\mathrm{i}}^2}}\begin{pmatrix} \beta_{\mathrm{r}} \\ \beta_{\mathrm{i}} \\ 0 \end{pmatrix} \tag{A15}$$

in which N_2 is a normalization factor. The corresponding eigenvalues are

$$\epsilon_1 = 0, \qquad \epsilon_2 = r - 3w^2, \qquad \epsilon_3 = 2R^2\beta_{\mathrm{r}}. \tag{A16}$$

Please note that the ψ_a in Eq. (A15) are the CLVs evaluated at $t = 0, T, \dots$ [namely, $c_a(0) = \psi_a$]. The CLVs at arbitrary time $c_a(t) \propto U(t)\psi_a$ are obtained by applying the evolution operator. In the case of periodic orbits, it is convenient to choose the phase to obtained time-periodic CLVs $c_a(t) = \mathrm{e}^{-it\epsilon_a}U(t)\psi_a = c_a(t + T)$.

We now look for the limits of ψ_i when $r \to 0$. We have $w = \pm\sqrt{r}$ when $r \to 0^+$ (from above), while $w = 0$ when $r \to 0^-$ (from below). The eigenvectors ψ_1 and ψ_3 do not depend on r, so we focus on ψ_2.

First case. Assume $h'(0) \neq 0$. In this case, we find that as $r \to 0$ (from above or below), $\psi_2 \to (0, 1, 0)$ provided that $\beta_{\mathrm{i}}\gamma_{\mathrm{r}} - \beta_{\mathrm{r}}\gamma_{\mathrm{i}} \neq 0$. [When this last condition is not met, $\psi_2 \to (1, h'(0)R\gamma_{\mathrm{i}}, -2\beta_{\mathrm{r}}R^2)/N_2$.]

Second case. When $h'(w) = w^\alpha$, the situation is more subtle. For $r < 0$, we always have $h' = 0$, so $\psi_2 \to (0, 0, 1)$ as $r \to 0^-$. For $r > 0$, $h' = r^{\alpha/2}$ and

$$\psi_2 = \frac{1}{N_2}\begin{pmatrix} r^{\alpha/2}R\gamma_{\mathrm{r}}(-2r) \\ r^{\alpha/2}R(\gamma_{\mathrm{i}}r + 2R^2(\beta_{\mathrm{i}}\gamma_{\mathrm{r}} - \beta_{\mathrm{r}}\gamma_{\mathrm{i}}) - 3\gamma_{\mathrm{i}}r) \\ 4r(r + \beta_{\mathrm{r}}R^2) \end{pmatrix}$$

$$\sim \frac{1}{N_2}\begin{pmatrix} C_1 r^{\alpha/2+1} \\ C_2 r^{\alpha/2} \\ C_3 r + 4r^2 \end{pmatrix} \tag{A17}$$

in which C_i are constants, N_2 ensures that the vector is normalized, and we have retained only the most important terms as $r \to 0$. In particular, $C_2 = 2R^3(\beta_{\mathrm{i}}\gamma_{\mathrm{r}} - \beta_{\mathrm{r}}\gamma_{\mathrm{i}})$ (we assume that this does not vanish) and $C_3 = -2\beta_{\mathrm{r}}R^2$. When $\alpha < 2$, $\psi_2 \to (0, 1, 0)$. When $\alpha = 2$ and $C_3 \neq 0$, $\psi_2 \to (0, C_2, C_3)/N_2$. When $\alpha > 2$ and $C_3 \neq 0$, $\psi_2 \to (0, 0, 1)$. When $C_3 = 0$, we have $\psi_2 \to (0, 1, 0)$ for $\alpha < 4$, $\psi_2 \to (0, C_2, 4)/N_2$ for $\alpha = 4$, and $\psi_2 \to (0, 0, 1)$ for $\alpha > 4$.

The conclusion of this calculation is that, except in higher-codimension submanifolds, we have $\psi_2 \to (0, 1, 0) = \psi_1$ (i.e., the Floquet vectors become parallel at the bifurcation) as $r \to 0^+$ provided that $h(w) \sim w^{\alpha+1}$ with $0 \leqslant \alpha < 2$. Besides, $\psi_2 \to (0, 1, 0) = \psi_1$ as $r \to 0^-$ when $h'(0) \neq 0$. In this case, the Floquet vectors become parallel from both sides, while in the other cases their behavior at the bifurcation is discontinuous.

APPENDIX B: $\mathbb{Z}_2$ SYMMETRIES

While no continuous symmetry is required for the tangency of covariant Lyapunov vector to happen (besides time translation invariance), some of the systems discussed in the main text have a discrete $\mathbb{Z}_2$ symmetry that interchanges the two stable attractors and leaves the unstable attractor (repellers) unchanged. In some cases, these symmetries are expressed as a time-dependent transformation. In this appendix, we discuss the general structure of these symmetries, and show how they emerge in the systems analyzed in the main text.

1. Standard and time-dependent symmetries

Consider a dynamical system

$$\dot{X} = f(X) \tag{B1}$$

in which $X(t) \in \mathbb{R}^N$ and a group G equipped with a group action $\rho : G \times \mathbb{R}^N \to \mathbb{R}^N$. We use the shorthand $g \cdot X = \rho(g, X)$ to refer to the action of a group element $g \in G$ on a vector $X \in \mathbb{R}^N$. The dynamical system is said to be equivariant with respect to the group G (more precisely, the group action ρ) when $f(g \cdot X) = g \cdot f(X)$ for all $g \in G$ and $X \in \mathbb{R}^N$. This guarantees that the equation of motion for the transformed variables $\tilde{Y} = g \cdot X$ are identical to the equations of motion for the original variables X. (In this Appendix, all tilded variables are transformed variables.) Namely, Eq. (B1) implies that $\dot{\tilde{X}} = f(\tilde{X})$.

Consider now a time-dependent "group action," so that the transformed variable is now $\tilde{X}(t) = \rho(t, g, X(t)) \equiv g(t) \cdot X(t)$. As an example, let us take a state $X \in \mathbb{R}^2$ represented (for convenience) as a complex number $z = X_1 + iX_2$ and the transformation $z(t) \mapsto \tilde{z}(t) = \mathrm{e}^{i\omega t}z^*(t)$ (the star denotes complex conjugation). Applying this transformation two times is gives back $z(t)$, so we can interpret it as defining a (time-dependent) representation of the group $\mathbb{Z}_2$ [187].

2. Systems analyzed in the main text

The pitchfork bifurcation (of fixed points) $\dot{w} = rw - w^3$ has a $\mathbb{Z}_2$ symmetry where the transformation is simply $\tilde{w} = -w$. Several of the systems analyzed in the main text have

a similar $\mathbb{Z}_2$ symmetry that either maps a steady state of the system to itself or interchanges two steady states:

The pitchfork of attractors Eq. (16b) is invariant under the transformation $w \mapsto \tilde{w} = -w$ when $g(x, w)$ is even in w [i.e., $g(x, -w) = g(x, w)$], with x left invariant by the transformation (i.e. $\tilde{x} = x$).

The Wilson-Cowan Eq. (30) is invariant under $\tilde{x}_i = -x_i$ when $h_i = 0$.

The predator-prey model in Eq. (31) is invariant under the transformation $\tilde{u}_1 = u_2, \tilde{v}_1 = v_2, \tilde{u}_2 = u_1, \tilde{v}_2 = v_1$ (because we have chosen identical parameters for the two prey-predator subsystems).

In all of these systems, the symmetry acts as a reflection interchanging the stable states, and leaving the unstable state invariant.

Other systems do not posses such a simple symmetry, but do exhibit a time-dependent Z_2 symmetry.

Consider the pitchfork of limit cycles (17). When $h(w) = w$, the frequency of the limit cycle depends on w, making a simple reflection ($\tilde{w} = -w, \tilde{z} = z$) insufficient: this transformation is not a symmetry, as it can be verified explicitly. Nevertheless, Eq. (17) has a time-dependent symmetry under certain conditions on the parameters. Consider the transformation

$$z \mapsto \tilde{z} = \mathrm{e}^{\mathrm{i}2\mathrm{Im}(\alpha)t} z^*,$$
$$w \mapsto \tilde{w} = -w. \tag{B2}$$

As in the case of a single pitchfork, the equation of motion for w is equivalent to the $\tilde{w}$ equation of motion. Let us now consider the other equation of motion. From the definition (B2) of $\tilde{z}$, we get

$$\dot{\tilde{z}} = (\dot{z}^* + \mathrm{i}2\mathrm{Im}(\alpha)z^*)\mathrm{e}^{\mathrm{i}2\mathrm{Im}(\alpha)t}. \tag{B3}$$

We start with the equation of motion (17) for z and complex conjugate it to obtain

$$\dot{z}^* = (\alpha^* + \beta^* |z|^2) z^* + \gamma^* h(w)z^*, \tag{B4a}$$

where we have used that $h(w) \in \mathbb{R}$. Hence,

$$\dot{\tilde{z}} = [(\alpha^* + \beta^* |z|^2) z^* + \gamma^* h(w)z^* + \mathrm{i}2\mathrm{Im}(\alpha)z^*]\mathrm{e}^{\mathrm{i}2\mathrm{Im}(\alpha)t} \tag{B5}$$

$$= [(\alpha^* + \beta^* |z|^2) + \gamma^* h(w) + \mathrm{i}2\mathrm{Im}(\alpha)]\tilde{z} \tag{B6}$$

$$= [(\alpha^* + \beta^* |\tilde{z}|^2) \pm \gamma^* h(\tilde{w}) + \mathrm{i}2\mathrm{Im}(\alpha)]\tilde{z}, \tag{B7}$$

where we have replaced $h(w)$ by $\pm h(\tilde{w}) = \pm h(-w) = h(w)$, where the $\pm$ depends on whether h is odd or even (cases where h is neither odd nor even are not considered). We have also used that $|\tilde{z}|^2 = |z|^2$. Assuming in addition that $\beta \in \mathbb{R}$ and that $\pm\gamma^* = \gamma$, we end up with

$$\dot{\tilde{z}} = [(\alpha^* + \mathrm{i}2\mathrm{Im}(\alpha) + \beta |\tilde{z}|^2) + \gamma h(\tilde{w})]\tilde{z} \tag{B8}$$

$$= [(\alpha + \beta |\tilde{z}|^2) + \gamma h(\tilde{w})]\tilde{z}. \tag{B9}$$

Hence, we have shown that the equation of motion for $(\tilde{z}, \tilde{w})$ is identical to the equation of motion for (z, w) provided that $\beta \in \mathbb{R}$ and $\gamma^* h(w) = \gamma h(-w)$.

Similarly, Eqs. (28) describing coupled nonlinear oscillators are invariant under the transformation

$$\begin{bmatrix} \tilde{z}_1 \\ \tilde{z}_2 \end{bmatrix} = \mathrm{e}^{\mathrm{i}2\omega t}\begin{bmatrix} z_1^* \\ z_2^* \end{bmatrix}. \tag{B10}$$

First, we have

$$\begin{bmatrix} \dot{\tilde{z}}_1 \\ \dot{\tilde{z}}_2 \end{bmatrix} = \mathrm{e}^{\mathrm{i}2\omega t}\begin{bmatrix} \dot{z}_1^* + \mathrm{i}2\omega z_1^* \\ \dot{z}_2^* + \mathrm{i}2\omega z_2^* \end{bmatrix}. \tag{B11}$$

Complex conjugating Eq. (28) yields

$$\begin{bmatrix} \dot{z}_1^* \\ \dot{z}_2^* \end{bmatrix} = \begin{bmatrix} (a - \mathrm{i}\omega) + b|z_1|^2 & a_{12} \\ a_{21} & (a - \mathrm{i}\omega) + b|z_2|^2 \end{bmatrix}\begin{bmatrix} z_1^* \\ z_2^* \end{bmatrix}, \tag{B12}$$

where we have assumed that $a, \omega, b, a_{12}, a_{21}$ are real. The two previous equations combine to give

$$\begin{bmatrix} \dot{\tilde{z}}_1 \\ \dot{\tilde{z}}_2 \end{bmatrix} = \mathrm{e}^{\mathrm{i}2\omega t}\begin{bmatrix} (a - \mathrm{i}\omega + \mathrm{i}2\omega) + b|z_1|^2 & a_{12} \\ a_{21} & (a - \mathrm{i}\omega + \mathrm{i}2\omega) + b|z_2|^2 \end{bmatrix}\begin{bmatrix} z_1^* \\ z_2^* \end{bmatrix} = \begin{bmatrix} (a + \mathrm{i}\omega) + b|\tilde{z}_1|^2 & a_{12} \\ a_{21} & (a + \mathrm{i}\omega) + b|\tilde{z}_2|^2 \end{bmatrix}\begin{bmatrix} \tilde{z}_1 \\ \tilde{z}_2 \end{bmatrix}. \tag{B13}$$

Therefore, the equations of motion are equivalent in both the $\tilde{z}$ and $\tilde{\tilde{z}}$ coordinate systems: Eq. (B10) is a time-dependent symmetry of Eq. (28) [when $a, \omega, b, a_{12}, a_{21} \in \mathbb{R}$].

The time-dependent symmetry transformations can be understood as the systems being invariant under complex conjugation in the rotating frame. The bifurcations of limit cycles analyzed in the main text fall in two classes:

(1) Systems with a time-independent $\mathbb{Z}_2$ symmetry (Wilson-Cowan model, Rosenzweig-MacArthur model), for which the CLVs are discontinuous at the bifurcation like Eq. (17) with $h(w) = w^2$,

(2) Systems with a time-dependent $\mathbb{Z}_2$ symmetry (coupled Hopf oscillators), for which the CLVs are continuous at the bifurcation, like Eq. (17) with $h(w) = w$.

It is not yet known whether the relation between the two classes of symmetry and the behaviors of the CLVs is general.

APPENDIX C: PITCHFORK OF TORI AND HIGHER-ORDER GENERALIZED EXCEPTIONAL POINTS

Higher-order generalized exceptional points and generalized exceptional points of limit tori can be constructed by modifying Eq. (17) to include additional Hopf oscillators and pitchfork bifurcations. We consider N Hopf oscillators indexed by $i = 1, \ldots, N$ and M pitchforks indexed by $j = 1, \ldots, M$. The Hopf oscillators are controlled by the
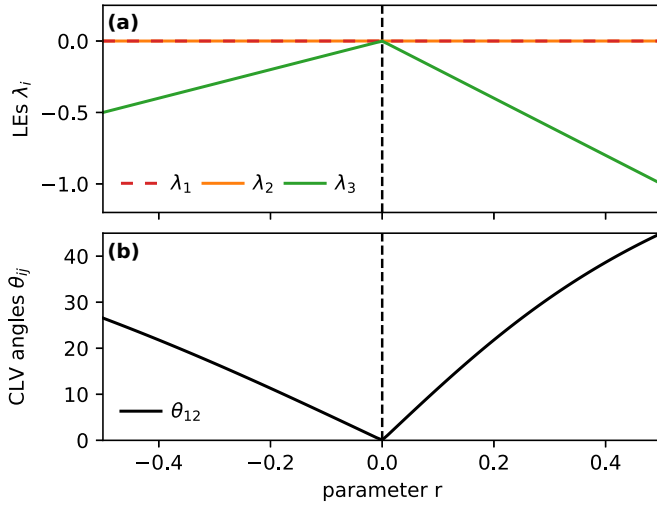
FIG. 12. Coalescence of CLVs in limit tori. In the main text, we have discussed the coalescence of CLVs in limit cycles (periodic evolutions). It is also possible to have a coalescence of CLVs in limit tori (a limit torus corresponds to a quasiperiodic evolution). This is illustrated using Eq. (C1) with parameters $M = 1$, $N = 2$, $\vec{\alpha} = (1 + i, 1/2 + i\pi)$, $\vec{\beta} = (-1, -1)$, $\vec{\gamma} = (i, 0)$, $\tau = 1$. The two highest Lyapunov exponents always vanish ($\lambda_1 = \lambda_2 = 0$, in red and orange in the top panel). At the critical value $r = 0$ of the control parameter, a third Lyapunov exponent λ_3 (in green) vanishes. The angle between the corresponding CLV c_3 and the two-dimensional vector space spanned by the CLVs c_1 and c_4 vanishes at $r = 0$ (bottom panel).

pitchforks as described by the dynamical system

$$\dot{z}_i = (\alpha_i + \beta_i |z_i|^2) z + \gamma_{ik} h(w_k),$$

$$\tau_j \dot{w}_j = r_i w_j - w_j^3, \tag{C1}$$

where γ_{ik} is the matrix of couplings of each oscillator to each pitchfork, and an implicit sum over k is taken. When $M = N = 1$, the system reduces to Eq. (17). When $M = 1$, $N > 1$ (i.e., we add additional Hopf oscillators) and at least one Hopf oscillator is adequately coupled to the pitchfork, the system will undergo a generalized exceptional point at the bifurcation of N-tori (under the conditions derived in Appendix A); see Fig. 12. As r approaches zero, the CLV corresponding to the pitchfork will approach a vector in the degenerate vector space spanned by the zero modes of each Hopf oscillator dependent on the exact choice of couplings. For the system in Eq. (C1), CLVs can be calculated by decomposing the system into Floquet problems for each Hopf oscillator, because the Hopf oscillators are decoupled from each other. By tuning multiple parameters, high-order generalized exceptional points can be found, where three or more CLVs align at once [188]. When $M > 1$ and $N = 1$ in Eq. (C1), if each pitchfork is adequately coupled to the Hopf oscillator and each r_i is simultaneously tuned to zero, then the CLV corresponding to each pitchfork will simultaneously align with the zero CLV of the Hopf oscillator producing an order-M generalized exceptional point (Fig. 13). While these examples are obtained by merely considering a product of independent dynamics, we expect that they occur at (relatively high codimension) bifurcations in generic dynamical systems.
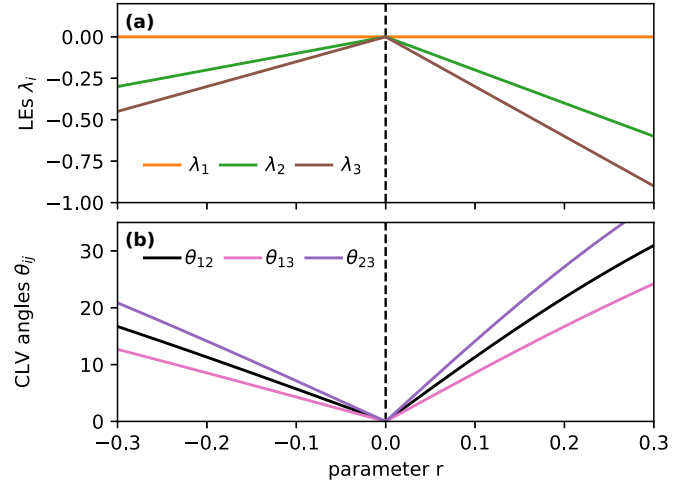

FIG. 13. Higher-order degeneracies. It is possible to have three (or more) covariant Lyapunov vectors becoming parallel at the same time. This generalizes higher-order exceptional point (an *n*th-order EP corresponds to *n* vectors becoming parallel, and to a Jordan block of size *n*). Here c_1, c_2, and c_3 all become parallel at $r = 0$. Equation (C1) with parameters $M = 2$, $N = 1$, $\alpha = 1 + i$, $\beta = -1$, $\gamma_j = (i, 2i)$, $\tau_j = (1, \frac{2}{3})$ causes three CLVs to merge at $r = 0$.

APPENDIX D: HYSTERESIS

In this appendix, we show that a nonlinear effect superficially similar to the dynamical encircling of exceptional points occurs when the symmetry between the attractors is explicitly broken. This may provide a mechanism for memory formation [189] in which the memory is stored in a dynamical state (a limit cycle, or a more complex attractor).

Consider encircling a generalized exceptional point in one of the systems analyzed in the main text. To do so, we may add a term $b w^2$ to Eq. (16b), so the pitchfork bifurcation becomes imperfect (like a paramagnetic/ferromagnetic transition under an external magnetic field). In this case, an effect superficially similar to the dynamical encircling of exceptional points occurs: the coalescence of attractors exhibits hysteresis. The effect is, however, fundamentally different: while the chiral mode conversion in linear systems is a purely dynamical effect, the number of steady-state solutions changes in a pitchfork of attractors when the parameters are varied.

In Fig. 14 we show that hysteresis emerges in the Wilson-Cowan system by varying the parameters in a closed loop around the bifurcation point, clockwise and counterclockwise. The external fields h_i break the $\mathbb{Z}_2$ symmetry of the Wilson-Cowan equations (see Appendix B).

APPENDIX E: GENERALIZED EXCEPTIONAL POINTS WITH NONZERO LYAPUNOV EXPONENTS

In the main text, we focus on generalized exceptional points (EP) with a vanishing Lyapunov exponent. In this appendix, we discuss generalized EP that have a nonzero Lyapunov exponent. As an example, Fig. 15 shows the Lyapunov exponents [Fig. 15(a)] and the angles between the corresponding covariant Lyapunov vectors [Fig. 15(b)] for the system of coupled nonlinear oscillators described by Eq. (28) and Fig. 8.
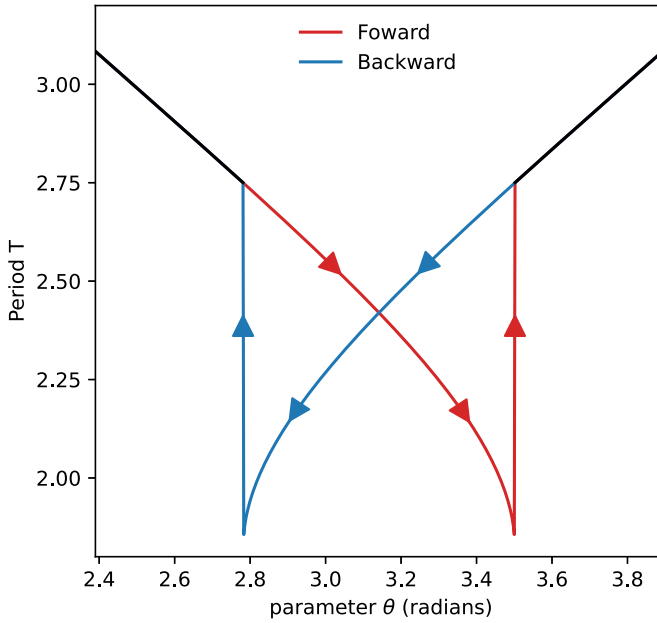
FIG. 14. Hysteresis. Hysteresis can be observed by adiabatically tuning the parameters around the exceptional point. We consider the Wilson-Cowan system with the same parameters as in Fig. 9. We set $\vec{h} = h(1, -1, 1)$ and choose the path encircling the EP $(\zeta, h) = (10.786 + 2\cos(\theta), 0.5\sin(\theta))$. We then let θ evolve either the clockwise (forward) or counterclockwise (backward) direction, and monitor the state of the system through the period T of the limit cycle. The paths coincide for part of the circle (black curves), but there is a region between $\theta \approx 2.75$ where the trajectories of the system on the forward (red) and backward (blue) path are different, signaling hysteresis.
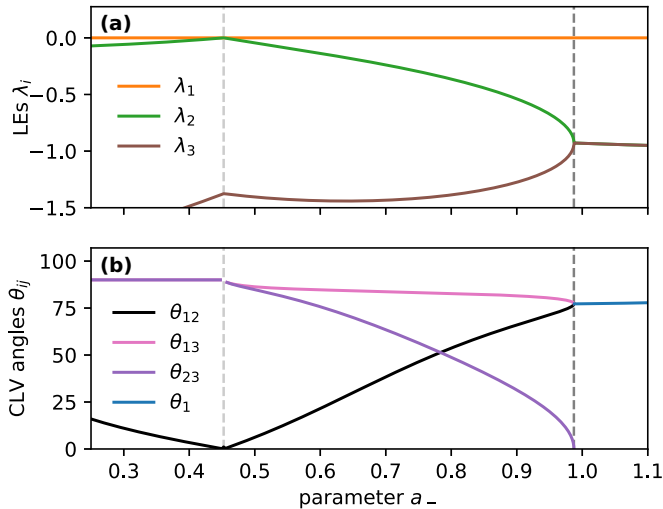

FIG. 15. Generalized exceptional point with a finite Lyapunov exponent. We simulate the coupled nonlinear oscillators given in Eq. (28). At the point $a_- = a_-^{\mathrm{f}} = 0.9872$ (dark gray dashed line), a nonzero Lyapunov exponent exceptional point occurs. In panel (a), the three smallest Lyapunov exponents are plotted. The angle θ_{23} between the CLVs c_2 and c_3 transitions from being aligned to being in a degenerate space. θ_1 is the angle from the CLV corresponding to λ_1 to the plane that contains the CLVs of λ_1 and λ_2 in the oscillatory region. We have set $a = \omega = -b = 1$, $a_+ = 0.1$. In panel (a), a_- is varied from 0.2 to 1.1.

We use the same parameters as in Figs. 8(e) and 8(f), with an extended range for the parameter a_-. As shown in Fig. 15, there is a generalized exceptional point with Lyapunov exponent $\lambda \sim -1$ at $a_-^{\mathrm{f}} \simeq 0.9872$.

In the case of limit cycles, insights about the effect of these generalized exceptional points can be gained using Floquet theory, see Appendix A 1. For $a_- > a_-^{\mathrm{f}}$, the two relevant Floquet exponents form a complex conjugate pair. Therefore, the CLVs form a degenerate subspace corresponding to the same Lyapunov exponents. For $a_- < a_-^{\mathrm{f}}$, the Floquet exponents have different magnitudes, so the Lyapunov exponents are different (the degeneracy is lifted). The generalized EP at a_-^{f} marks a change in the transient behavior of the system similar to the transition from overdamped to underdamped oscillations towards a fixed point. In the case of a periodic orbit, Floquet theory allows us to decompose the evolution of a perturbation $\delta X(0)$ into two parts by writing $U(t) = V(t)e^{tF}$ where $V(t + T) = V(t)$; see Appendix A 1. The periodic part corresponds to $V(t)$, while the nonperiodic part corresponds to F (the eigenvalues of which are the Floquet exponents), and can be measured by performing stroboscopic measurements of $\delta X(t)$ (i.e., measuring it every period). This nonperiodic part of the evolution describes the overall relaxation towards the limit cycle, which can be monotonic or oscillatory.

APPENDIX F: ESTIMATION OF THE PHASE DIFFUSION CONSTANT

In this appendix, we provide details about the effect of noise in the solvable model discussed in the main text. We estimate the phase diffusion constant in for Ornstein-Uhlenbeck noise (away from the generalized exceptional point) in Sec. F1, a quartic potential using results from Ref. [190] in Sec. F2, and higher dimensional analogues of the quartic potential in Sec. F3.

1. Integrated Ornstein-Uhlenbeck process

We consider the set of coupled stochastic differential equations

$$\mathrm{d}x_t = -a\, x_t\, \mathrm{d}t + \sigma\, \mathrm{d}W_t, \tag{F1a}$$

$$\mathrm{d}y_t = \omega_1\, x_t\, \mathrm{d}t \tag{F1b}$$

in which W_t is a standard Wiener process and $\sigma \equiv \sqrt{2T}$. With $x \sim w$ and $y \sim \phi$, they correspond to a version of Eqs. (23) of the main text where the nonlinear term w^3 has been removed and $\omega_0 = 0$. (This gives a rough idea of the behavior of the system when r is large enough for the nonlinear term to be mostly negligible, which is far from the generalized exceptional point.) Our goal is to evaluate the variance of the integral y_t of the Ornstein-Uhlenbeck process $x_t \equiv x(t)$.

The stationary distribution associated with the SDE above is

$$p(x) = \mathcal{N}e^{-V(x)/T}, \tag{F2}$$

where $V(x) = ax^2/2$ and $\mathcal{N}$ is a normalization factor such that p integrates to unity. In addition, the mean and covariance of

the stationary (unconditioned) process are

$$\mathbb{E}[x_t] = 0,$$

$$\text{cov}(x_s, x_t) \equiv \mathbb{E}[(x_s - \mathbb{E}[x_s])(x_t - \mathbb{E}[x_t])]$$

$$= \mathbb{E}[x_s x_t] = \frac{\sigma^2}{2a} e^{-a|t-s|}. \tag{F3}$$

In particuliar the variance of x_t is $\frac{\sigma^2}{2a} = \frac{T}{a}$.

We now estimate the variance of y_t. Integrating the SDE, we find

$$y_t = \omega_1 \int_0^t x(s) \mathrm{d}s. \tag{F4}$$

Therefore, we have

$$\mathbb{E}[y_t] = \omega_1 \int_0^t \mathbb{E}[x(s)] ds = 0 \tag{F5}$$

and

$$\mathbb{E}[y_t^2] = \omega_1^2 \mathbb{E}\left[\left(\int_0^t x(r) dr\right)\left(\int_0^t x(s) ds\right)\right]$$

$$= \omega_1^2 \int_0^t dr \int_0^t ds \mathbb{E}[x(r)x(s)]$$

$$= \omega_1^2 \frac{\sigma^2}{2a} \frac{2}{a^2}(at + e^{-at} - 1) \sim \omega_1^2 \frac{\sigma^2}{a^2} t \tag{F6}$$

in which we have used the expression of the covariance Eq. (F3) and the property

$$\int_0^t dr \int_0^t ds e^{-\alpha|r-s|} = \frac{2}{\alpha^2}(\alpha t + e^{-\alpha t} - 1) \underset{\alpha t \gg 1}{\sim} \frac{2}{\alpha} t \tag{F7}$$

with $\alpha = a$. From Eq. (F6), we obtain the effective diffusion coefficient quoted in the main text for a process y_t submitted to an Ornstein-Uhlenbeck noise x_t.

2. Integrated quartic-potential noise

We now consider the situation in which the quartic potential of the Ornstein-Uhlenbeck process is replaced with a quartic potential. This occurs in Eq. (23) as we approach the generalized exceptional point. The stochastic differential equations are

$$dx_t = \left(-ax_t - bx_t^3\right)dt + \sigma \, dW_t = -V'(x_t) \, dt + \sigma \, dW_t, \tag{F8a}$$

$$dy_t = \omega_1 x_t \, dt \tag{F8b}$$

with $\sigma = \sqrt{2T}$. Again, our goal is to evaluate the variance of y_t. These equations correspond to Eqs. (23) with $x \sim w$ and $y \sim \phi$ (and $\omega_0 = 0$). In contrast with the previous section, we did not remove the nonlinear term (w^3 or x^3). The potential in Eq. (F8) is

$$V(x) = \tfrac{1}{2}ax^2 + \tfrac{1}{4}bx^4. \tag{F9}$$

Here, we consider the case where the quartic potential has a single minimum (i.e., it is not a double-well potential) that corresponds on one side of the bifurcation (the handle side of the pitchfork). Similar calculations can be performed on the other side of the bifurcation [190]. The stationary distribution is

$$p(x) = \mathcal{N}e^{-V(x)/T} \qquad \text{where} \qquad \mathcal{N} = \frac{\pi}{2}\sqrt{\frac{|a|}{b}}e^{\frac{a^2}{8bT}}\left[I_{-1/4}\left(\frac{a^2}{8bT}\right) - \frac{a}{|a|}I_{1/4}\left(\frac{a^2}{8bT}\right)\right] \tag{F10}$$

in which $I_n(z)$ is the modified Bessel function of the first kind of order n [[191], Sec. 10.25].

Computing the moments yields the mean and the variance

$$\mathbb{E}[x_t] = 0 \qquad \text{and} \qquad \text{Var}[x_t] = \frac{T}{2|a|}\frac{\{z^2[I_{5/4}(z^2/4) - I_{3/4}(z^2/4)] + (z^2 + 2)I_{1/4}(z^2/4) - z^2 I_{-1/4}(z^2/4)\}}{[I_{-1/4}(z^2/4) - (a/|a|)I_{1/4}(z^2/4)]}, \tag{F11}$$

where we have defined $z \equiv a/\sqrt{2bT}$.

We will be interested in the limit $a \to 0$, and it is enough for our purposes to consider the case $a = 0^+$. Computing the limit yields

$$\text{Var}[x_t; a = 0^+] = \langle x_t^2 \rangle = \sqrt{\frac{T}{b}}\frac{\sqrt{2}\,\Gamma^2(3/4)}{\pi} \tag{F12}$$

in which Γ is the Euler gamma function [[191], Sec. 5.2].

Chapter 6 of Ref. [190] gives an analytic expression for the correlation function. Combined with the variance in Eq. (F12), this gives the covariance of x_t, from which we will obtain the variance of y_t. For small enough a (i.e., small z) the covariance is reasonably approximated by the simple expression [190]

$$\langle x_t x_s \rangle = \langle x_t^2 \rangle e^{-t/T_c} \tag{F13}$$

in which T_c is the correlation time (defined as the area under the curve of the normalized autocorrelation function), that can in turn be approximated as

$$T_c(q) = \tau_0 \frac{e^q - 1}{2q}(\pi\sqrt{q} + 2^{1-\sqrt{q}}), \tag{F14}$$

where $q = z^2/2$ and $\tau_0 = 1/\sqrt{2bT}$. When $a = 0$ (i.e.. $z = 0$ and $q = 0$), one has

$$\frac{T_c}{\tau_0} = \frac{\Gamma^2(1/4)}{4\sqrt{2\pi}}[\pi - 2\log(\sqrt{2} + 1)] \simeq 1.01989\ldots. \tag{F15}$$
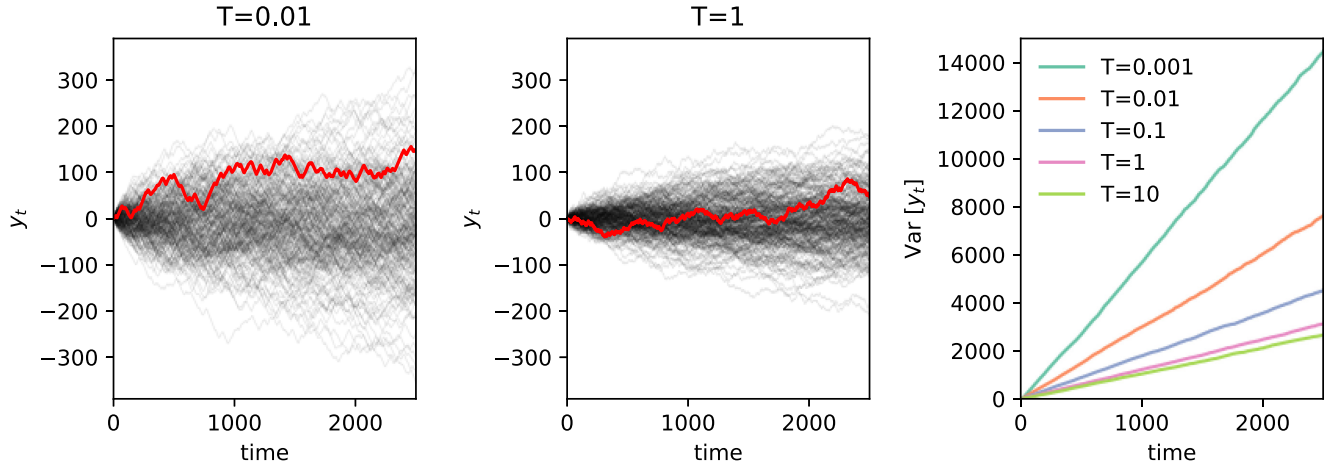
FIG. 16. Diffusion at a third-order generalized exceptional point in a nonlinear potential. We demonstrate diffusion for Eq. (F18) with $a_2 = 0$, $\sigma_1 = 0$, and all remaining unspecified constants set equal to one. The left and middle panels show an ensemble of y_t trajectories at $T = 0.01$ and $T = 1$, respectively, with an example trajectory highlighted in red. The rightmost panel plots the variance of y_t over time at various temperatures.

Hence, we get in the limit $a = 0^+$ and when t is large compared to T_c

$$\text{Var}[y_t] = \mathbb{E}[y_t^2] = \omega_1^2 \int_0^t dr \int_0^t ds \, \langle x(r)x(s) \rangle$$

$$\underset{t \gg T_c}{\sim} \left[\frac{2\,\Gamma^2(3/4)}{\pi} \right] \left[\frac{T_c}{\tau_0} \right] \omega_1^2 \frac{1}{b} t \tag{F16}$$

using Eq. (F12) and Eq. (F7) with $\alpha = 1/T_c$. In the limit $a \to 0$, the quantity T_c/τ_0 is given in Eq. (F15). This gives the effective diffusion coefficient quoted in the main text (Sec. IV C 1).

At arbitrary a, the variance is given by

$$\text{Var}[y_t] = \mathbb{E}[y_t^2] = \omega_1^2 \int_0^t dr \int_0^t ds \, \langle x(r)x(s) \rangle$$

$$\underset{t \gg T_c}{\sim} \left[\frac{T_c}{\tau_0} \right] \sqrt{\frac{2}{bT}} \omega_1^2 \langle x_t^2 \rangle t. \tag{F17}$$

For $a < 0$, the diffusion coefficient monotonically decreases in temperature until the critical temperature scale $T_{crit} \approx a^2/4b$, implying the system diffuses *more slowly* with greater noise intensity. While unintuitive, this can be understood as follows: In the telegraph noise regime, the y variable behaves as a one-dimensional active particle undergoing diffusion with mean free path length $\approx \tau^* \omega_1 \sqrt{a/b}$ where τ^* is given by Eq. (27). Lower temperatures lead to longer mean-free paths and faster diffusion. Diffusion at the exceptional point arises as the marginal behavior between active and Brownian diffusion.

3. A higher-dimensional example

Consider the coupled stochastic differential equations

$$dy_t = \omega_1 x_t \, dt, \tag{F18a}$$

$$dx_t = (a_1 w_t - b_1 x_t^3) dt + \sigma_1 dW_t^x, \tag{F18b}$$

$$dw_t = (a_2 x_t - b_2 w_t^3) dt + \sigma_2 dW_t^w, \tag{F18c}$$

where we assume $b_1 > 0$ and $b_2 > 0$ for stability. In higher dimensional examples at exceptional points of order $\geqslant 3$, we find the system still diffuses more slowly with greater noise intensity even though the system is unistable, which precludes an explanation in terms of telegraph noise. In Fig. 16 we show numerical simulations of Eq. (F18) that exhibit a diffusion coefficient scaling inversely with temperature.

The diffusion at the third-order exceptional point exhibits similar scaling with temperature in the situation where $a_1 = a_2 < 0$ (we call a their common value), which admits similar telegraph noise as above. The equations become

$$dy_t = \omega_1 x_t \, dt, \tag{F19a}$$

$$dx_t = -\partial_x V \, dt + \sigma \, dW_t^x, \tag{F19b}$$

$$dw_t = -\partial_w V \, dt + \sigma \, dW_t^w, \tag{F19c}$$

where

$$V(x, w) = \tfrac{1}{4} b_1 x^4 + a x w + \tfrac{1}{4} b_2 w^4. \tag{F20}$$

The stationary distribution is given by

$p(x) = \mathcal{N} e^{-V(x)/T}$ where

$$\mathcal{N} = \frac{\pi^2 |a|}{2\sqrt{2b_1 b_2}} \left[I_{-1/4}\left(\frac{a^2}{4T\sqrt{b_1 b_2}} \right)^2 + I_{1/4}\left(\frac{a^2}{4T\sqrt{b_1 b_2}} \right)^2 \right] \tag{F21}$$

in which $I_n(z)$ is the modified Bessel function of the first kind of order n [[191], Sec. 10.25].

From this, we find the variance of x_t with respect to the steady state distribution to be

$$\text{Var}[x_t] = \frac{1}{\mathcal{N}} \frac{\sqrt{2\pi} T e^{\frac{a^2}{2T\sqrt{b_1 b_2}}}}{\sqrt[4]{b_1^3 b_2}}. \tag{F22}$$

Importantly, the equation contains the factor $e^{\frac{a^2}{2T\sqrt{b_1 b_2}}}$ which is nonanalytic in T, b_1, b_2 and therefore inaccessible through perturbation theory. We again use the approximate time correlation expression (F13), but due to the system now being

two-dimensional, there is no identical exact solution for the correlation time. Instead we use the approximation found in [190]

$$T_c \approx -\frac{C_x(0)}{\dot{C}_x(0)} \tag{F23}$$

in which $C_x(0) = \text{Var}[x_0]$ and $\dot{C}_x(0) = \mathbb{E}[x_0 \frac{dx_0}{dt}] = \mathbb{E}[x_0(aw_0 - b_1 x_0^3)]$. Taking the expectation with the steady state distribution, we find

$$\mathbb{E}[x_0(aw_0 - b_1 x_0^3)] = -T, \tag{F24}$$

and finally, the diffusion of y_t is found to be

$$\begin{aligned}
\text{Var}[y_t] &= \mathbb{E}[y_t^2] \\
&= \omega_1^2 \int_0^t dr \int_0^t ds \, \langle x(r)x(s) \rangle \underset{t \gg T_c}{\sim} 2\omega_1^2 \langle x_t^2 \rangle^2 \frac{t}{T} \quad \text{(F25)} \\
&= \frac{32\omega_1^2 \sqrt{\frac{b_2}{b_1}} T e^{\frac{a^2}{T\sqrt{b_1 b_2}}}}{\pi^2 a^2 \left[I_{-1/4}\left(\frac{a^2}{4T\sqrt{b_1 b_2}}\right)^2 + I_{1/4}\left(\frac{a^2}{4T\sqrt{b_1 b_2}}\right)^2 \right]^2} t \\
&\underset{T \to \infty}{\sim} \frac{4\Gamma\left(\frac{3}{4}\right)^4 \omega_1^2}{\pi^2 b_1} t. \quad \text{(F26)}
\end{aligned}$$

The diffusion constant (F26) is monotonically decreasing in temperature for $a < 0$ towards a finite value equal to the integrated quartic-potential diffusion constant up to a numerical coefficient.

4. Analysis of the plankton food web model

In this appendix, we analyze a set of coupled Rosenzweig-MacArthur-like equations used in Ref. [175] to model laboratory experiments on a plankton food web isolated from the Baltic Sea [29]. Following these references, we consider N_{pred} consumers (predators) feeding on N_{prey} resources (prey). The populations $u_i(t)$ of resources and $v_k(t)$ of consumers evolve according to

$$\frac{du_i}{dt} = r_i u_i \left(1 - \sum_{j=1}^{N_{\text{prey}}} \frac{u_j \alpha_{ij}}{K_i}\right) - \sum_{k=1}^{N_{\text{pred}}} \frac{g_k u_i v_k \beta_{ik}}{\sum_{j=1}^{N_{\text{prey}}} u_j \beta_{jk} + H_k}, \tag{F27a}$$

$$\frac{dv_k}{dt} = \frac{g_k v_k \left(\sum_{j=1}^{N_{\text{prey}}} u_j \beta_{jk}\right)}{\sum_{j=1}^{N_{\text{prey}}} u_j \beta_{j,k} + H_k} - m_k v_k. \tag{F27b}$$

Here we take $N_{\text{pred}} = N_{\text{prey}} = 2$ (so the state of the system is described by $X \equiv (u_1, u_2, v_1, v_2)$), and $r_1 = r_2 = 1$, $K_1 = K_2 = 1$, $m_1 = m_2 = m \simeq 0.12$, $g_1 = g_2 = g \simeq 1.5$, $H_1 = H_2 = H \simeq 1.1$, $\alpha_{11} = \alpha_{22} = 1$, $\alpha_{12} = \alpha_{21} = \alpha \simeq 1.2$, $\beta_{11} = \beta_{22} = 1$, $\beta_{12} = \beta_{21} = \beta$. The parameter β quantifies the coupling through predation and is taken as a bifurcation parameter. For these values, we find that a bifurcation takes place at $\beta_c \simeq 0.02275$. We have slightly modified the numerical values used in Ref. [175] without crossing any bifurcation in order to make the system less stiff, and the calculations of the LEs and CLVs easier. We take as initial conditions $X(0) \equiv (u_1(0), u_2(0), v_1(0), v_2(0)) = (0.5, 0.1, 0.5, 0.5)$ and $(0.1, 0.5, 0.5, 0.5)$. For the parameters considered, these are in the basin of attraction of the only limit cycle below the

bifurcation [Figs. 11(a)–11(c)], and in the respective basins of attractions of the two stable limit cycles above the bifurcation [Figs. 11(d)–11(i)].

A direct integration of Eqs. (F27) is performed using a LSODA approach with automatic switching between a nonstiff Adams method and a stiff BDF method as implemented in Mathematica NDSolve. The numerical integration is carried out for a long number of periods (of the order of 5000 periods) in order to obtain a good approximation $X(t)$ of the limit cycle. A precise estimation of the period T is obtained by tracking the extrema of $u_i(t)$ using a Brent-Dekker root-finding method as implemented by Mathematica WhenEvent. We then solve

$$\delta\dot{U} = J(X(t))U \tag{F28}$$

with initial condition $U(0) = \text{Id}$ (Id is the identity matrix) from $t = 0$ to $t = T$, in which the Jacobian of the vector field defined by the right-hand side of Eqs. (F27) is computed analytically. Evaluating the solution $U(t)$ at the final time gives the Floquet operator $U(T)$.

Diagonalizing the Floquet operator $U(T)$ produces eigenvalues μ_i and eigenvectors $\vec{w}_i$. The LEs are identified as $\lambda_i = \log |\mu_i|$, while the CLVs at time $t = 0$ (modulo a period) are $\vec{c}_i(0) = \vec{w}_i$, perhaps up to a normalization. We then apply the evolution operator $U(t)$ to find $\vec{c}_i(t) = U(t)\vec{c}_i(0)$. Finally, we compute the angles $\theta_{ij}(t)$ between the CLVs, that satisfy $\cos\theta_{ij}(t) = \vec{c}_i(t) \cdot \vec{c}_j(t)/[\|\vec{c}_i(t)\| \|\vec{c}_j(t)\|]$. We emphasize that these angles depend on time. In order to quantify how align are the CLVs, we compute the average of $[\sin\theta_{ij}(t)]^2$ over one period.

Typical trajectories are shown in Figs. 11(a)–11(i). We observe that below a critical value $\beta_c \simeq 0.02275$ of the parameter β describing coupling through predation, a single limit cycle exists, with the two predators in antiphase (as well as the prey); see Figs. 11(a)–11(c). As shown in Fig. 11(c), the projections of the cycle in the (u_1, v_1) and (u_2, v_2) planes are identical. For $\beta > \beta_c$, two limit cycles are present, with the two predators oscillating with a dephasing $\delta\phi$ that is neither zero nor π [Figs. 11(d)–11(i)]. Figures 11(f) and 11(i) show that the projections of each cycle on the (u_1, v_1) and (u_2, v_2) planes are now different, and the roles of both populations are exchanged between the two limit cycles. We plot as a function of β the two Lyapunov exponent closest to zero ($\lambda_1 \equiv 0$ and λ_2) in Fig. 11(j) and the average angle between the corresponding covariant vectors in Fig. 11(k) (more precisely, we plot the average $\langle \sin^2(\theta_{12}) \rangle$ over one period, in which θ_{12} is the angle between the CLV $\vec{c}_i$ ($i = 1, 2$), because only the directions corresponding to the CLVs are physically meaningful, so $\pm\vec{c}_i$ are equivalent). We find that the Lyapunov exponents vanish at the bifurcation. The angle θ_{12} between the CLVs also vanishes, and its behavior is discontinuous from the left through the bifurcation. Figure 11(l) shows the dephasing between the predator densities. Finally, Fig. 11(m) shows the instantaneous quantity $\sin^2\theta_{12}(t)$ over one period for different values of β. We observe that the angle between the CLVs depends on the location on the periodic orbit. Even away from the generalized EP, small values of the angles may occur at some points of the limit cycle. For $\beta \to \beta_c^+$, the instantaneous angle $\theta_{12}(t)$ becomes arbitrarily small all along the limit cycle (black curve).
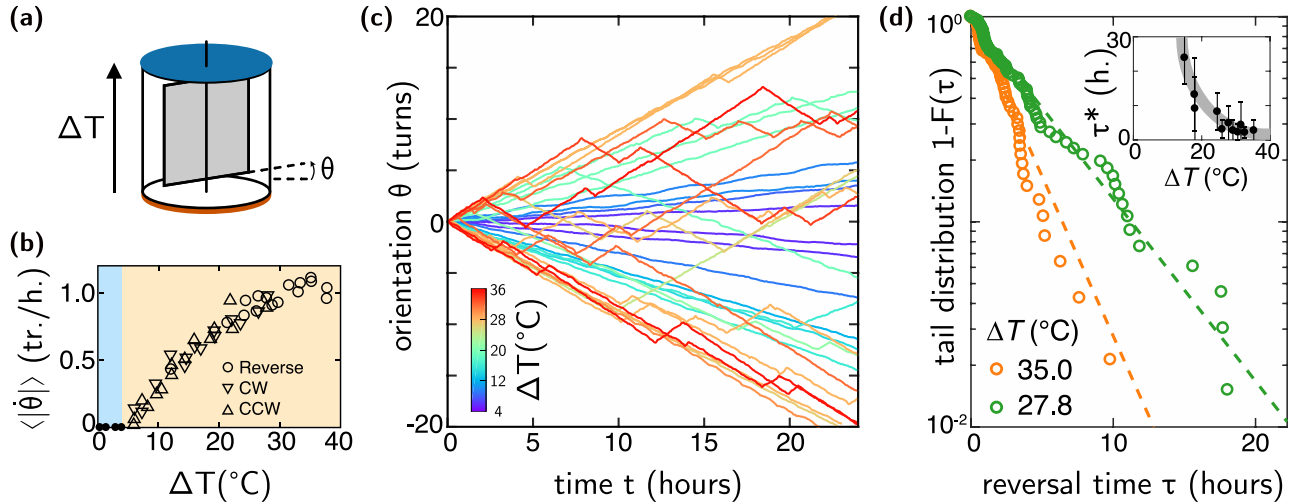
FIG. 17. Free rotation of a solid body in Rayleigh-Bénard convection. We reproduce from Ref. [30] figures summarizing their experimental results. (a) Description of the system: a temperature gradient ΔT is applied to a cylindrical convection cell containing a solid body freely rotating about the axis of the cylinder. The angular position θ of the body with respect to a fixed axis is recorded. (b) When ΔT is increased, the system bifurcates from a state with no average rotation to a state with finite average rotation speed. The magnitude of the rotation speed is determined by ΔT (it is approximately a square root of the distance to threshold) but its sign is random. (c) Observation of time series of the angle θ in the high-ΔT regime shows that there are frequent reversals of the rotation: the system switches between clockwise and counterclockwise motion. (d) The distribution of sojour times in the (counter)clockwise states is approximately exponential, as evidenced by the tail distribution [$F(\tau)$ is the cumulative distribution; the probability density function is $p(\tau) = F'(\tau)$]. Dashed lines are fits by $F(\tau) = 1 - \exp(-\tau/\tau^*)$. Panels (b)–(d) are adapted from [30].

APPENDIX G: EXPERIMENTAL EXAMPLE: FREE ROTATION OF A SOLID BODY IN A CONVECTION CELL

As an illustration of the integrated telegraphic noise discussed in Sec. IV C 2, we now compare in Fig. 17 the predictions of the normal form Eq. (23) to experimental results from Ref. [30]. In this work, a plate is immersed in a cylindrical convection cell. The plate can freely rotate about the axis of the cylinder. A temperature gradient ΔT is imposed between the top and bottom of the cell, leading to Rayleigh-Bénard convection. The rotation of the plate due to its interaction with the fluctuating flow is then monitored through its angle θ with a fixed axis. At low temperature gradients, the average rotation rate $\langle|\dot{\theta}|\rangle$ vanishes. As ΔT passes a critical value ΔT_c, the average rotation rate $\langle|\dot{\theta}|\rangle$ becomes finite. In this regime, reversals in the sign of the rotation rate are observed, and are reported to follow a Poisson process.

Rather than performing a first-principles model of this experimental situation and trying to reduce it, we make a guess and directly identify $r = (\Delta T - \Delta T_c)/\Delta T_c$ in Eq. (23). Our simple model then reproduces the experimentally observed (i) square-root-like behavior of $\langle|\dot{\theta}|\rangle$ with ΔT, (ii) the two classes of behavior in time of θ (compare panels (e) and (f) of Fig. 7 with the two regimes [in blue and red, respectively] in panel (c) of Fig. 17) and (iii) the Poissonian distribution of the reversal times.

[1] S. Shankar, A. Souslov, M. J. Bowick, M. C. Marchetti, and V. Vitelli, Topological active matter, Nat. Rev. Phys. 4, 380 (2022).

[2] Y. Ashida, Z. Gong, and M. Ueda, Non-Hermitian physics, Adv. Phys. 69, 249 (2020).

[3] H. Nassar, B. Yousefzadeh, R. Fleury, M. Ruzzene, A. Alù, C. Daraio, A. N. Norris, G. Huang, and M. R. Haberman, Nonreciprocity in acoustic and elastic materials, Nat. Rev. Mater. 5, 667 (2020).

[4] E. J. Bergholtz, J. C. Budich, and F. K. Kunst, Exceptional topology of non-Hermitian systems, Rev. Mod. Phys. 93, 015005 (2021).

[5] A. Clerk, Introduction to quantum non-reciprocal interactions: from non-Hermitian Hamiltonians to quantum master equations and quantum feedforward schemes, SciPost Phys. Lect. Notes 44 (2022).

[6] M. Fruchart, C. Scheibner, and V. Vitelli, Odd viscosity and odd elasticity, Annu. Rev. Condens. Matter Phys. 14, 471 (2023).

[7] T. Kato, Perturbation Theory for Linear Operators, 2nd ed. (Springer, Berlin, Heidelberg, 1984).

[8] L. D. Landau and E. M. Lifshitz, Mechanics: Volume 1 (Butterworth Heinemann, Oxford, 1976).

[9] M.-A. Miri and A. Alù, Exceptional points in optics and photonics, Science 363, eaar7709 (2019).

[10] L. N. Trefethen and M. Embree, Spectra and Pseudospectra: The Behavior of Nonnormal Matrices and Operators (Princeton University Press, Princeton, 2005).

[11] A. Ghatak, M. Brandenbourger, J. van Wezel, and C. Coulais, Observation of non-Hermitian topology and its bulk–edge correspondence in an active mechanical metamaterial, Proc. Natl. Acad. Sci. USA **117**, 29561 (2020).

[12] P. Baconnier, D. Shohat, C. H. López, C. Coulais, V. Démery, G. Düring, and O. Dauchot, Selective and collective actuation in active solids, Nat. Phys. **18**, 1234 (2022).

[13] T. Tlusty, Exceptional topology in ordinary soft matter, Phys. Rev. E **104**, 025002 (2021).

[14] J. Wiersig, Review of exceptional point-based sensors, Photon. Res. **8**, 1457 (2020).

[15] J. Doppler, A. A. Mailybaev, J. Böhm, U. Kuhl, A. Girschik, F. Libisch, T. J. Milburn, P. Rabl, N. Moiseyev, and S. Rotter, Dynamically encircling an exceptional point for asymmetric mode switching, Nature (London) **537**, 76 (2016).

[16] A. U. Hassan, B. Zhen, M. Soljačić, M. Khajavikhan, and D. N. Christodoulides, Dynamically encircling exceptional points: Exact evolution and polarization state conversion, Phys. Rev. Lett. **118**, 093002 (2017).

[17] C. Dembowski, B. Dietz, H.-D. Gräf, H. L. Harney, A. Heine, W. D. Heiss, and A. Richter, Encircling an exceptional point, Phys. Rev. E **69**, 056216 (2004).

[18] S. Strogatz, *Nonlinear Dynamics and Chaos: With Applications to Physics, Biology, Chemistry, and Engineering* (Chapman & Hall Book, CRC Press, Boca Raton, 2019).

[19] P. Manneville, *Instabilities, Chaos and Turbulence*, ICP Fluid Mechanics (Imperial College Press, London, 2010).

[20] J. D. Murray, *Mathematical Biology: I. An Introduction*, Interdisciplinary Applied Mathematics (Springer, New York, 2013).

[21] M. Golubitsky and D. G. Schaeffer, *Singularities and Groups in Bifurcation Theory* (Springer, New York, 1985), Vol. I.

[22] M. Golubitsky, I. Stewart, and D. G. Schaeffer, *Singularities and Groups in Bifurcation Theory* (Springer, New York, 1988), Vol. II.

[23] M. Golubitsky and I. Stewart, *The Symmetry Perspective* (Birkhäuser, Basel, 2002).

[24] J. D. Crawford and E. Knobloch, Symmetry and symmetry-breaking bifurcations in fluid dynamics, Annu. Rev. Fluid Mech. **23**, 341 (1991).

[25] S. P. Timoshenko and J. M. Gere, *Theory of Elastic Stability*, Dover Civil and Mechanical Engineering (Dover Publications, Mineola, 2009).

[26] M. Fruchart, R. Hanai, P. B. Littlewood, and V. Vitelli, Nonreciprocal phase transitions, Nature (London) **592**, 363 (2021).

[27] A. Pikovsky and A. Politi, *Lyapunov Exponents: A Tool to Explore Complex Dynamics* (Cambridge University Press, Cambridge, 2016).

[28] J. P. Eckmann and D. Ruelle, Ergodic theory of chaos and strange attractors, Rev. Mod. Phys. **57**, 617 (1985).

[29] E. Benincà, J. Huisman, R. Heerkloss, K. D. Jöhnk, P. Branco, E. H. Van Nes, M. Scheffer, and S. P. Ellner, Chaos in a long-term experiment with a plankton community, Nature (London) **451**, 822 (2008).

[30] K. Wang and J. Zhang, Persistent corotation of the large-scale flow of thermal convection and an immersed free body, Proc. Natl. Acad. Sci. USA **120**, e2217705120 (2023).

[31] Technically, $\delta X(t)$ is a tangent vector, i.e., an element of the tangent space to the unperturbed trajectory at point $X(t)$. For a fixed point, $X(t) = X_0$.

[32] A. P. Seyranian, O. N. Kirillov, and A. A. Mailybaev, Coupling of eigenvalues of complex matrices at diabolic and exceptional points, J. Phys. A: Math. Gen. **38**, 1723 (2005).

[33] S. Lang, *Linear Algebra*, Undergraduate Texts in Mathematics (Springer, New York, 2010).

[34] Y. A. Kuznetsov, *Elements of Applied Bifurcation Theory* (Springer, New York, 2004).

[35] A. D. Bazykin, *Nonlinear Dynamics of Interacting Populations*, World Scientific Series on Nonlinear Science, Series A, Monographs and Treatises (World Scientific, Singapore, 1998), Vol. 11.

[36] E. M. Izhikevich, *Dynamical Systems in Neuroscience* (MIT Press, Cambridge, 2007).

[37] Y. Y. Renardy, M. Renardy, and K. Fujimura, Takens–Bogdanov bifurcation on the hexagonal lattice for double-layer convection, Physica D **129**, 171 (1999).

[38] L. Jaeger and H. Kantz, Homoclinic tangencies and non-normal Jacobians—Effects of noise in nonhyperbolic chaotic systems, Physica D **105**, 79 (1997).

[39] T. Biancalani, F. Jafarpour, and N. Goldenfeld, Giant amplification of noise in fluctuation-induced pattern formation, Phys. Rev. Lett. **118**, 018101 (2017).

[40] R. Chajwa, N. Menon, S. Ramaswamy, and R. Govindarajan, Waves, algebraic growth, and clumping in sedimenting disk arrays, Phys. Rev. X **10**, 041016 (2020).

[41] The same is true for repellers and similar isolated structures, and our discussion also applies to these cases.

[42] Formally, the evolution operator $U(t, t_0)$ is defined as the unique solution of the Cauchy problem (6) with $\delta X(t_0) = \mathrm{Id}$, with Id the identity matrix. It is also known as the fundamental matrix of Eq. (6).

[43] J. J. Sakurai, *Modern Quantum Mechanics* (Addison Wesley, Reading, 1993).

[44] M. Le Bellac, *Quantum Physics* (Cambridge University Press, Cambridge, 2012).

[45] P. V. Kuptsov and U. Parlitz, Theory and computation of covariant Lyapunov vectors, J. Nonlinear Sci. **22**, 727 (2012).

[46] P. Gaspard and J. R. Dorfman, Chaotic scattering theory, thermodynamic formalism, and transport coefficients, Phys. Rev. E **52**, 3525 (1995).

[47] F. Ginelli, P. Poggi, A. Turchi, H. Chaté, R. Livi, and A. Politi, Characterizing dynamics with covariant Lyapunov vectors, Phys. Rev. Lett. **99**, 130601 (2007).

[48] S. Schubert and V. Lucarini, Covariant Lyapunov vectors of a quasi-geostrophic baroclinic model: Analysis of instabilities and feedbacks, Q. J. R. Meteorol. Soc. **141**, 3040 (2015).

[49] We refer the reader to [55,112], which include a discussion of degenerate cases.

[50] C. L. Wolfe and R. M. Samelson, An efficient method for recovering Lyapunov vectors from singular vectors, Tellus A: Dyn. Meteorol. Oceanog. **59**, 355 (2007).

[51] F. Ginelli, H. Chaté, R. Livi, and A. Politi, Covariant Lyapunov vectors, J. Phys. A: Math. Theor. **46**, 254005 (2013).

[52] K. A. Takeuchi and H. Chaté, Collective Lyapunov modes, J. Phys. A: Math. Theor. **46**, 254007 (2013).

[53] H.-L. Yang and G. Radons, Comparison between covariant and orthogonal Lyapunov vectors, Phys. Rev. E **82**, 046204 (2010).

[54] G. Froyland, T. Hüls, G. P. Morriss, and T. M. Watson, Computing covariant Lyapunov vectors, Oseledets vectors,

and dichotomy projectors: A comparative numerical study, Physica D **247**, 18 (2013).

[55] A. Trevisan and F. Pancotti, Periodic orbits, Lyapunov vectors, and singular vectors in the Lorenz system, J. Atmos. Sci. **55**, 390 (1998).

[56] F. Noethen, A projector-based convergence proof of the Ginelli algorithm for covariant Lyapunov vectors, Physica D **396**, 18 (2019).

[57] W. E. Wiesel, Continuous time algorithm for Lyapunov exponents. I, Phys. Rev. E **47**, 3686 (1993).

[58] W. E. Wiesel, Continuous time algorithm for Lyapunov exponents. II, Phys. Rev. E **47**, 3692 (1993).

[59] B. Hejazi, B. Mehlig, and G. A. Voth, Emergent scar lines in chaotic advection of passive directors, Phys. Rev. Fluids **2**, 124501 (2017).

[60] G. A. Voth, G. Haller, and J. P. Gollub, Experimental measurements of stretching fields in fluid mixing, Phys. Rev. Lett. **88**, 254501 (2002).

[61] L. Arnold, D. C. Nguyen, and V. Oseledets, Jordan normal form for linear cocycles, Random Oper. and Stock. Equ. **7**, 303 (1999).

[62] C. González-Tokman and A. Quas, Multiplicative ergodic theorems and applications, CMS Notes **45** (2013).

[63] Two remarks are in order. First, it is possible to have equal Lyapunov exponents with different CLVs (a trivial example consists in two identical decoupled dynamical systems, considered as a single dynamical system). Conversely, two identical CLVs must have the same Lyapunov exponent (because they are the same vector; this is a tautology).

[64] In the main text, all the examples we consider correspond to a Jordan block of size two. The case of higher-order singularities is discussed in Appendix C.

[65] In general, the angles between CLVs depend on time (equivalently, on the base point on the trajectory). However, two CLVs that are exactly parallel at one point are also exactly parallel along the whole trajectory. In order to illustrate the presence of a tangency in the examples, we either average the angles θ_{ij} between the CLVs $\vec{c}_i$ and $\vec{c}_j$ over the trajectory, or, in the case of (quasi)periodic dynamics we evaluate them at a distinguished point (e.g., where an arbitrary coordinate is maximal). See Appendix F 4 [in particular Fig. 11(m)] for an example.

[66] H.-L. Yang, K. A. Takeuchi, F. Ginelli, H. Chaté, and G. Radons, Hyperbolicity and the effective dimension of spatially extended dissipative systems, Phys. Rev. Lett. **102**, 074102 (2009).

[67] K. A. Takeuchi, H. liu Yang, F. Ginelli, G. Radons, and H. Chaté, Hyperbolic decoupling of tangent space and effective dimension of dissipative systems, Phys. Rev. E **84**, 046214 (2011).

[68] N. Sharafi, M. Timme, and S. Hallerberg, Critical transitions and perturbation growth directions, Phys. Rev. E **96**, 032220 (2017).

[69] M. Xu and M. R. Paul, Covariant Lyapunov vectors of chaotic Rayleigh-Bénard convection, Phys. Rev. E **93**, 062208 (2016).

[70] H. Bosetti and H. A. Posch, Covariant Lyapunov vectors for rigid disk systems, Chem. Phys. **375**, 296 (2010).

[71] S. Vannitsem and V. Lucarini, Statistical and dynamical properties of covariant Lyapunov vectors in a coupled atmosphere-ocean model—Multiscale effects, geometric degeneracy, and error dynamics, J. Phys. A: Math. Theor. **49**, 224001 (2016).

[72] Consider, for instance, the matrix.

$$J(\epsilon) = \begin{pmatrix} \sigma & \epsilon \\ 1 - \epsilon & \sigma \end{pmatrix}. \tag{6.29}$$

This matrix has exceptional points $\epsilon = 0$ and $\epsilon = 1$. Consider now the linear dynamical system $\dot{X} = J(\epsilon)X \equiv f_\epsilon(X)$ for $X \in \mathbb{R}^2$. It has a unique fixed point at $X = 0$. In the case of a fixed points, the CLVs are the eigenvectors of the Jacobian [here $J(\epsilon)$], so there is indeed a tangency of the CLVs at $\epsilon = 0$ (and at $\epsilon = 1$). The fixed point $X = 0$ does change nature at $\epsilon = 0$ from a node (for $\epsilon = 0^-$, where the streamlines of the vector field are essentially straight), to a focus (for $\epsilon = 0^+$, where the streamlines are spiraling). Nevertheless, the dynamical systems at $\epsilon = 0^\pm$ are topologically equivalent (see, for instance, Example 2.1 in Ref. [34]), so there is no bifurcation.

[73] E. Knobloch, J. Hettel, and G. Dangelmayr, Parity breaking bifurcation in inhomogeneous systems, Phys. Rev. Lett. **74**, 4839 (1995).

[74] Up to a non-linear change of variable, the circle and line can be mapped to arbitrary closed and open curves.

[75] P. Coullet and S. Fauve, Propagative phase dynamics for systems with Galilean invariance, Phys. Rev. Lett. **55**, 2857 (1985).

[76] P. Coullet, R. E. Goldstein, and G. H. Gunaratne, Parity-breaking transitions of modulated patterns in hydrodynamic systems, Phys. Rev. Lett. **63**, 1954 (1989).

[77] B. Malomed and M. Tribelsky, Bifurcations in distributed kinetic systems with aperiodic instability, Physica D **14**, 67 (1984).

[78] S. Douady, S. Fauve, and O. Thual, Oscillatory phase modulation of parametrically forced surface waves, Europhys. Lett. **10**, 309 (1989).

[79] M. E. Brachet, P. Coullet, and S. Fauve, Propagative phase dynamics in temporally intermittent systems, Europhys. Lett. **4**, 1017 (1987).

[80] L. Pan and J. R. de Bruyn, Spatially uniform traveling cellular patterns at a driven interface, Phys. Rev. E **49**, 483 (1994).

[81] D. Bensimon, A. Pumir, and B. Shraiman, Nonlinear theory of traveling wave convection in binary mixtures, J. Phys. France **50**, 3089 (1989).

[82] S. Xin, P. Le Quéré, and L. S. Tuckerman, Bifurcation analysis of double-diffusive convection with opposing horizontal thermal and solutal gradients, Phys. Fluids **10**, 850 (1998).

[83] U. Thiele, K. John, and M. Bär, Dynamical model for chemically driven running droplets, Phys. Rev. Lett. **93**, 027802 (2004).

[84] M. Kness, L. S. Tuckerman, and D. Barkley, Symmetry-breaking bifurcations in one-dimensional excitable media, Phys. Rev. A **46**, 5054 (1992).

[85] K. Krischer and A. Mikhailov, Bifurcation to traveling spots in reaction-diffusion systems, Phys. Rev. Lett. **73**, 3165 (1994).

[86] A. U. Hassan, H. Hodaei, M.-A. Miri, M. Khajavikhan, and D. N. Christodoulides, Nonlinear reversal of the $\mathcal{PT}$-symmetric phase transition in a system of coupled semiconductor microring resonators, Phys. Rev. A **92**, 063807 (2015).

[87] E. Clerkin, S. O'Brien, and A. Amann, Multistabilities and symmetry-broken one-color and two-color states in closely coupled single-mode lasers, Phys. Rev. E **89**, 032919 (2014).

[88] M. C. Soriano, J. García-Ojalvo, C. R. Mirasso, and I. Fischer, Complex photonics: Dynamics and applications of delay-coupled semiconductors lasers, Rev. Mod. Phys. **85**, 421 (2013).

[89] H. Hong and S. H. Strogatz, Kuramoto model of coupled oscillators with positive and negative coupling parameters: An example of conformist and contrarian oscillators, Phys. Rev. Lett. **106**, 054102 (2011).

[90] H. Hong and S. H. Strogatz, Conformists and contrarians in a Kuramoto model with identical natural frequencies, Phys. Rev. E **84**, 046202 (2011).

[91] H. Hong, Periodic synchronization and chimera in conformist and contrarian oscillators, Phys. Rev. E **89**, 062924 (2014).

[92] M. Leonetti, J. Nuebler, and F. Homble, Parity-breaking bifurcation and global oscillation in patterns of ion channels, Phys. Rev. Lett. **96**, 218101 (2006).

[93] R. Hanai, A. Edelman, Y. Ohashi, and P. B. Littlewood, Non-Hermitian phase transition from a polariton Bose-Einstein condensate to a photon laser, Phys. Rev. Lett. **122**, 185301 (2019).

[94] R. Hanai and P. B. Littlewood, Critical fluctuations at a many-body exceptional point, Phys. Rev. Res. **2**, 033018 (2020).

[95] S. Saha, J. Agudo-Canalejo, and R. Golestanian, Scalar active mixtures: The nonreciprocal Cahn-Hilliard model, Phys. Rev. X **10**, 041009 (2020).

[96] Z. You, A. Baskaran, and M. C. Marchetti, Nonreciprocity as a generic route to traveling states, Proc. Natl. Acad. Sci. USA **117**, 19767 (2020).

[97] T. Frohoff-Hülsmann, M. P. Holl, E. Knobloch, S. V. Gurevich, and U. Thiele, Stationary broken parity states in active matter models, Phys. Rev. E **107**, 064210 (2023).

[98] L. Ophaus, S. V. Gurevich, and U. Thiele, Resting and traveling localized states in an active phase-field-crystal model, Phys. Rev. E **98**, 022608 (2018).

[99] It is interesting to compare the parity-breaking bifurcation to the Bogdanov-Takens bifurcation [34], typically associated with a nondiagonalizable Jacobian. Despite having the same linear part (corresponding to the nondiagonalizable Jacobian), their nonlinear parts do not match. This is because the dynamical system (13) does not satisfy the genericity conditions that are usually assumed to obtain the normal form of the Bogdanov-Takens bifurcation [Eqs. (BT.0-3) in Theorem 8.4 of Ref. [34], for instance]. The parity breaking can then be thought as a degenerate version of a Bogdanov-Takens bifurcation (see Ref. [192] and references therein for other similar situations).

[100] Let p be the vector of parameters needed to parameterize $f(x; p)$. We can choose a function $\pi(w)$ and set $p = \pi(w)$. By choosing a reference parameter p_0 and setting $g(x, w) = f(x; \pi(w)) - f(x; p_0)$, and $f(x) = f(x; p_0)$, we go back to the case discussed in the main text.

[101] Here we assume that a limit cycle occurs on both sides of the bifurcation. This is not necessarily the case. Setting $\alpha = \beta = 0$ and $h(w) = w$, we find that Eq. (18) reduces to the normal form of the parity-breaking bifurcation (13), in which a fixed point exists on one side, and two limit cycles on the other side.

[102] E. V. Nikolaev and E. E. Shnol, Bifurcations of cycles in systems of differential equations with a finite symmetry group—I, J. Dyn. Control Syst. **4**, 315 (1998).

[103] E. V. Nikolaev and E. E. Shnol, Bifurcations of cycles in systems of differential equations with a finite symmetry group—II, J. Dyn. Control Syst. **4**, 343 (1998).

[104] E. V. Nikolaev, Bifurcations of limit cycles of differential equations admitting an involutive symmetry, Sb. Math. **186**, 611 (1995).

[105] J. Abshagen, J. M. Lopez, F. Marques, and G. Pfister, Mode competition of rotating waves in reflection-symmetric Taylor–Couette flow, J. Fluid Mech. **540**, 269 (2005).

[106] M. G. Pedersen, M. Brøns, and M. P. Sørensen, Amplitude-modulated spiking as a novel route to bursting: Coupling-induced mixed-mode oscillations by symmetry breaking, Chaos **32**, 013121 (2022).

[107] A. Sherman, Anti-phase, asymmetric and aperiodic oscillations in excitable cells—I. Coupled bursters, Bull. Math. Biol. **56**, 811 (1994).

[108] A. Röhm, K. Lüdge, and I. Schneider, Bistability in two simple symmetrically coupled oscillators with symmetry-broken amplitude- and phase-locking, Chaos **28**, 063114 (2018).

[109] F. Marques, F. Mellibovsky, and A. Meseguer, Fold-pitchfork bifurcation for maps with Z_2 symmetry in pipe flow, Phys. Rev. E **88**, 013006 (2013).

[110] I. Bačić and I. Franović, Two paradigmatic scenarios for inverse stochastic resonance, Chaos **30**, 033123 (2020).

[111] A. R. Willms, P. M. Kitanov, and W. F. Langford, Huygens' clocks revisited, R. Soc. Open Sci. **4**, 170777 (2017).

[112] F. Huhn and L. Magri, Stability, sensitivity and optimisation of chaotic acoustic oscillations, J. Fluid Mech. **882**, A24 (2019).

[113] E. N. Lorenz, Deterministic nonperiodic flow, J. Atmos. Sci. **20**, 130 (1963).

[114] E. Ott, *Chaos in Dynamical Systems* (Cambridge University Press, Cambridge, 2002).

[115] The model (21) does not directly describes coupled chaotic attractors. The parallels between this situation and the case of limit cycles suggest that a bifurcation accompanied by a coalescence of covariant Lyapunov attractors could occur in coupled chaotic attractors, maybe in relation with their synchronization [193,194]. However, this is not analyzed in this work. Relations between Lyapunov vectors and attractor merging crises [195–197], which occur when attractors collide with each, other have also been put forward [198,199].

[116] C. Rackauckas and Q. Nie, DifferentialEquations.jl—A performant and feature-rich ecosystem for solving differential equations in Julia, J. Open Res. Softw. **5**, 15 (2017).

[117] G. Benettin, L. Galgani, A. Giorgilli, and J.-M. Strelcyn, Lyapunov characteristic exponents for smooth dynamical systems and for hamiltonian systems: A method for computing all of them. Part 1: Theory, Meccanica **15**, 9 (1980).

[118] G. Benettin, L. Galgani, A. Giorgilli, and J.-M. Strelcyn, Lyapunov characteristic exponents for smooth dynamical systems and for Hamiltonian systems: A method for computing all of them. Part 2: Numerical application, Meccanica **15**, 21 (1980).

[119] T. Frohoff-Hülsmann, J. Wrembel, and U. Thiele, Suppression of coarsening and emergence of oscillatory behavior in a Cahn-Hilliard model with nonvariational coupling, Phys. Rev. E **103**, 042602 (2021).

[120] L. Ophaus, E. Knobloch, S. V. Gurevich, and U. Thiele, Two-dimensional localized states in an active phase-field-crystal model, Phys. Rev. E **103**, 032601 (2021).

[121] E. Knobloch, Spatial localization in dissipative systems, Annu. Rev. Condens. Matter Phys. **6**, 325 (2015).

[122] L. Brusch, M. G. Zimmermann, M. van Hecke, M. Bär, and A. Torcini, Modulated amplitude waves and the transition from phase to defect chaos, Phys. Rev. Lett. **85**, 86 (2000).

[123] M. A. Muñoz, Colloquium: Criticality and dynamical scaling in living systems, Rev. Mod. Phys. **90**, 031001 (2018).

[124] Lyapunov exponent are asymptotic quantities describing the growth rate at large times. By definition, they do not pick up the transient effects we discuss here. These can be captured more easily by so-called finite-time Lyapunov exponents and similar quantities. It is remarkable that the long-time CLVs are still a partial proxy for some transient effects.

[125] In general, there can be several missing directions $\vec{c}_n^{\perp}$. At an exceptional point, these would correspond to so-called generalized eigenvectors in the Jordan decomposition of a matrix. Note also that in the figure, the tangent space is shown as light-gray squares orthogonal to the black trajectory for graphical reasons; in practice, CLVs can be tangent to the trajectory.

[126] Y. Kuramoto, *Chemical Oscillations, Waves, and Turbulence* (Springer, Berlin, Heidelberg, 1984).

[127] A. T. Winfree, *The Geometry of Biological Time* (Springer, New York, 2001).

[128] J. Guckenheimer, Isochrons and phaseless sets, J. Math. Biol. **1**, 259 (1975).

[129] A. T. Winfree, Patterns of phase compromise in biological cycles, J. Math. Biol. **1**, 73 (1974).

[130] F. Dumortier, Asymptotic phase and invariant foliations near periodic orbits, Proc. Am. Math. Soc. **134**, 2989 (2006).

[131] C. Chicone and W. Liu, Asymptotic phase revisited, J. Diff. Equ. **204**, 227 (2004).

[132] A. Mauroy and I. Mezić, On the use of Fourier averages to compute the global isochrons of (quasi)periodic dynamics, Chaos **22**, 033112 (2012).

[133] A. Mauroy, I. Mezić, and J. Moehlis, Isostables, isochrons, and Koopman spectrum for the action–angle representation of stable fixed point dynamics, Physica D **261**, 19 (2013).

[134] A. Mauroy and I. Mezic, Global stability analysis using the eigenfunctions of the Koopman operator, IEEE Trans. Automat. Contr. **61**, 3356 (2016).

[135] N. Ichinose, K. Aihara, and K. Judd, Extending the concept of isochrons from oscillatory to excitable systems for modeling an excitable neuron, Int. J. Bifurc. Chaos **08**, 2375 (1998).

[136] S. Shirasaka, W. Kurebayashi, and H. Nakao, Phase-amplitude reduction of transient dynamics far from attractors for limit-cycling systems, Chaos **27**, 023119 (2017).

[137] D. Wilson and J. Moehlis, Extending phase reduction to excitable media: Theory and applications, SIAM Rev. **57**, 201 (2015).

[138] K. M. Shaw, Y.-M. Park, H. J. Chiel, and P. J. Thomas, Phase resetting in an asymptotically phaseless system: On the phase response of limit cycles verging on a heteroclinic orbit, SIAM J. Appl. Dyn. Syst. **11**, 350 (2012).

[139] M. G. Rosenblum, A. S. Pikovsky, and J. Kurths, Phase synchronization of chaotic oscillators, Phys. Rev. Lett. **76**, 1804 (1996).

[140] J. T. C. Schwabedal, A. Pikovsky, B. Kralemann, and M. Rosenblum, Optimal phase description of chaotic oscillators, Phys. Rev. E **85**, 026216 (2012).

[141] R. Tönjes and H. Kori, Phase and frequency linear response theory for hyperbolic chaotic oscillators, Chaos **32**, 043124 (2022).

[142] G. Himona, V. Kovanis, and Y. Kominis, Isochrons, phase response and synchronization dynamics of tunable photonic oscillators, Phys. Rev. Res. **4**, L012039 (2022).

[143] H. Nakao, T. Yanagita, and Y. Kawamura, Phase-reduction approach to synchronization of spatiotemporal rhythms in reaction-diffusion systems, Phys. Rev. X **4**, 021032 (2014).

[144] In Ref. [128], it is proven that isochrons exist under the hypothesis that the limit cycle is hyperbolic (this means that the only Floquet multiplier on the unit circle corresponds to the Floquet eigenvector $\vec{c}_*$ with multiplier $\mu = 1$; see Ref. [34]). Nonhyperbolic limit cycles typically have no well-defined isochrons, but this is not necessarily true [200,201]. Conversely, limit cycles without well-defined isochrons are necessarily nonhyperbolic. This is because the hyperbolicity is defined in terms of Floquet multipliers (or Lyapunov exponents), while the existence or absence of isochrons is related to the Floquet eigenvectors (or CLVs). Namely, the isochrons cannot be well defined when another CLV aligns with $\vec{c}_*$. For instance, an exactly solvable planar system without isochrons can be found in Ref. [145], in which the monodromy matrix [Eq. (13) in the reference] is a Jordan block of size two. We also refer to Refs. [202–204] for a discussion of the effect of noise on an oscillator with twisted isochrons from the point of view of so-called Ruelle-Pollicott resonances.

[145] A. Demir, Fully nonlinear oscillator noise analysis: An oscillator with no asymptotic phase, Int. J. Circuit Theory Appl. **35**, 175 (2007).

[146] B. Lindner, Diffusion coefficient of a brownian particle with a friction function given by a power law, J. Stat. Phys. **130**, 523 (2008).

[147] B. Lindner and E. M. Nicola, Diffusion in different models of active Brownian motion, Eur. Phys. J. Spec. Top. **157**, 43 (2008).

[148] B. Lindner and E. M. Nicola, Critical asymmetry for giant diffusion of active Brownian particles, Phys. Rev. Lett. **101**, 190603 (2008).

[149] P. Romanczuk, M. Bär, W. Ebeling, B. Lindner, and L. Schimansky-Geier, Active Brownian particles: From individual to collective stochastic dynamics, Eur. Phys. J. Spec. Top. **202**, 1 (2012).

[150] If we assume that the phase correlations are eventually diffusive [namely, $\langle \phi(t_0 + t)\phi(t_0)\rangle \sim Dt$], these results can be guessed by dimensional analysis. To do so, let us consider the SDEs $dw = rw\,dt - bw^3 + \sigma\,dW$ and $d\phi = \omega_1 w$ in which W is a Wiener process. We attribute independent dimensions $[w] = \mathsf{W}$ and $[\phi] = \Phi$ to the variables w and ϕ (here, square brackets label the dimension of a quantity). In addition, the dimension symbol of time is T. The parameters are $[r] = \mathsf{T}^{-1}$, $[b] = \mathsf{T}^{-1}\mathsf{W}^{-2}$, $[\omega_1] = \Phi\mathsf{W}^{-1}\mathsf{T}^{-1}$, and $[\sigma] = \mathsf{W}\mathsf{T}^{-1/2}$ (recall that $[dW] = \sqrt{[dt]}$). In addition, the diffusion coefficient we are looking for has dimension $[D] = \Phi^2\mathsf{T}^{-1}$. First, assume $b = 0$ (and $r \neq 0$); dimensional analysis yields that the only combination of parameters with the appropriate dimension is $[D] = [\omega_1^2\sigma^2/r^2]$, so $D \sim \sigma^2 \sim T_w$. Second, assume $r = 0$ (and $b \neq 0$); in the same way, dimensional analysis yields $[D] = [\omega_1^2/b]$ which does not depend on the noise strength

σ^2 (i.e., on the temperature T_w). A similar analysis can be performed when $d\phi = \omega_1^{(2)} w^2$ (this corresponds to the case of Sec. II C with discontinuous CLVs); in this case, we find that dimensionally, $D \sim [\omega_1^{(2)}]^2 \sigma b^{-3/2} \sim \sqrt{T_w}$. We can therefore expect a significant increase of fluctuations near the bifurcation compared to the case far from the exceptional point where $r \gg b$ at low T_w. The general case in which both r and b are finite is not fully determined by dimensional analysis. We refer to Ref. [205] for a more complete scaling theory.

[151] More precisely, the time evolution of w can be approximated as a discrete-state continuous-time Markov process with two states $w_{\pm}$ [corresponding to the two minima of $U(w)$] with transition rates $1/\tau^*$ between the states following the master equation.

$$\partial_t \begin{pmatrix} p_+ \\ p_- \end{pmatrix} = \begin{pmatrix} -\lambda_{-+} & \lambda_{+-} \\ \lambda_{-+} & -\lambda_{+-} \end{pmatrix} \begin{pmatrix} p_+ \\ p_- \end{pmatrix} \qquad (6.30)$$

in which $\lambda_{ij} = \lambda_{j \to i}$ is the rate of transition from i to j, given by $\lambda_{+-} = \lambda_{-+} = 1/\tau^*$ as the double well is symmetric. As the transition rates are constant, the distribution of waiting times is exponential, reproducing Eq. (25). The telegraph noise is also known as a burst noise, a Markovian dichotomous noise, or a Kac process. It is related to a Poisson process in the sense that the number of changes between the two states in an interval of duration τ is Poissonian. See Refs. [157–159] for details. We also note that a superposition of a large number of random telegraph processes can produce a $1/f$ noise [206,207].

[152] P. Hänggi, P. Talkner, and M. Borkovec, Reaction-rate theory: Fifty years after Kramers, Rev. Mod. Phys. **62**, 251 (1990).

[153] N. Berglund, Kramers' law: Validity, derivations and generalisations, Markov Processes Relat. Fields **19**, 459 (2013).

[154] A. Bovier, M. Eckhoff, V. Gayrard, and M. Klein, Metastability in reversible diffusion processes I: Sharp asymptotics for capacities and exit times, J. Eur. Math. Soc. **6**, 399 (2004).

[155] A. Bovier, V. Gayrard, and M. Klein, Metastability in reversible diffusion processes II: Precise asymptotics for small eigenvalues, J. Eur. Math. Soc. **7**, 69 (2005).

[156] F. Bouchet and J. Reygner, Generalisation of the Eyring–Kramers transition rate formula to irreversible diffusion processes, Ann. Henri Poincaré **17**, 3499 (2016).

[157] N. V. Kampen, *Stochastic Processes in Physics and Chemistry* (Elsevier, 1992).

[158] W. Horsthemke and R. Lefever, *Noise-Induced Transitions* (Springer-Verlag, Berlin, Heidelberg, 2006).

[159] I. Bena, Dichotomous Markov noise: Exact results for out-of-equilibrium systems, Int. J. Mod. Phys. B **20**, 2825 (2006).

[160] P. Hänggi and P. Jung, Colored noise in dynamical systems, Adv. Chem. Phys. **89**, 239 (1995).

[161] G. H. Weiss, Some applications of persistent random walks and the telegrapher's equation, Physica A **311**, 381 (2002).

[162] J. Masoliver and K. Lindenberg, Continuous time persistent random walk: A review and some generalizations, Eur. Phys. J. B **90**, 107 (2017).

[163] R. Kutner and J. Masoliver, The continuous time random walk, still trendy: Fifty-year history, state of art and outlook, Eur. Phys. J. B **90**, 50 (2017).

[164] J. Tailleur and M. E. Cates, Statistical mechanics of interacting run-and-tumble bacteria, Phys. Rev. Lett. **100**, 218103 (2008).

[165] L. Touzo, P. L. Doussal, and G. Schehr, Interacting, running and tumbling: The active Dyson Brownian motion, Europhys. Lett. **142**, 61004 (2023).

[166] H. Haken, *Synergetics: An Introduction*, Springer Series in Synergetics (Springer, Berlin, Heidelberg, 1983).

[167] H. R. Wilson and J. D. Cowan, Excitatory and inhibitory interactions in localized populations of model neurons, Biophys. J. **12**, 1 (1972).

[168] A. Pérez-Cervera, P. Ashwin, G. Huguet, T. M. Seara, and J. Rankin, The uncoupling limit of identical Hopf bifurcations with an application to perceptual bistability, J. Math. Neurosci. **9**, 7 (2019).

[169] J. Rankin, E. Sussman, and J. Rinzel, Neuromechanistic model of auditory bistability, PLoS Comput. Biol. **11**, e1004555 (2015).

[170] D. Pressnitzer and J.-M. Hupé, Temporal dynamics of auditory and visual bistability reveal common principles of perceptual organization, Curr. Biol. **16**, 1351 (2006).

[171] F. Macpherson and K. Wilson, Bistable Auditory Stimulus, https://www.illusionsindex.org/i/bistable-auditory-stimulus, archived at https://web.archive.org/web/20250426084009/https://www.illusionsindex.org/i/bistable-auditory-stimulus.

[172] J. Vandermeer, Oscillating populations and biodiversity maintenance, BioScience **56**, 967 (2006).

[173] P. Chesson, Mechanisms of maintenance of species diversity, Annu. Rev. Ecol. Systematics **31**, 343 (2000).

[174] R. A. Armstrong and R. McGehee, Competitive exclusion, Amer. Naturalist **115**, 151 (1980).

[175] E. Benincà, K. D. Jöhnk, R. Heerkloss, and J. Huisman, Coupled predator-prey oscillations in a chaotic food web, Ecol. Lett. **12**, 1367 (2009).

[176] P. Turchin, *Complex Population Dynamics: A Theoretical/Empirical Synthesis (MPB-35)*, Monographs in Population Biology (Princeton University Press, Princeton, 2013).

[177] J. Maynard-Smith, *Models in Ecology* (Cambridge University Press, Cambridge, 1978).

[178] M. L. Rosenzweig and R. H. MacArthur, Graphical representation and stability conditions of predator-prey interactions, Am. Naturalist **97**, 209 (1963).

[179] J. Vandermeer, Coupled oscillations in food webs: Balancing competition and mutualism in simple ecological models, Am. Naturalist **163**, 857 (2004).

[180] J. Vandermeer, Loose coupling of predator-prey cycles: Entrainment, chaos, and intermittency in the classic macarthur consumer-resource equations, Am. Natur. **141**, 687 (1993).

[181] C. Xue and N. Goldenfeld, Coevolution maintains diversity in the stochastic "kill the winner" model, Phys. Rev. Lett. **119**, 268101 (2017).

[182] D. J. Luitz and F. Piazza, Exceptional points and the topology of quantum many-body spectra, Phys. Rev. Res. **1**, 033051 (2019).

[183] Zenodo, https://doi.org/10.5281/zenodo.15699799.

[184] G. Floquet, Sur les équations différentielles linéaires à coefficients périodiques, Ann. Sci. École Norm. Sup. **12**, 47 (1883).

[185] A. M. Lyapunov, Problème général de la stabilité du mouvement, Ann. Fac. Sci. Toulouse **9**, 203 (1907).

[186] G. Teschl, *Ordinary Differential Equations and Dynamical Systems* (American Mathematical Society, Providence, 2012).

[187] To be more precise, let ± 1 represent the two elements of $\mathbb{Z}_2$ (viewed multiplicatively), then we define $\rho(t, -1, z(t)) = e^{i\omega t} z^*(t)$ and $\rho(t, +1, z(t)) = z(t)$.

[188] In linear algebra, an exceptional point of order n corresponds to a Jordan block of size n. For instance, the canonical Jordan block of size three associated with the eigenvalue λ has the form

$$\begin{pmatrix} \lambda & 1 & 0 \\ 0 & \lambda & 1 \\ 0 & 0 & \lambda \end{pmatrix}.$$

We refer to Refs. [61,62] for the equivalent notion in the case of covariant Lyapunov vectors.

[189] N. C. Keim, J. D. Paulsen, Z. Zeravcic, S. Sastry, and S. R. Nagel, Memory formation in matter, Rev. Mod. Phys. **91**, 035002 (2019).

[190] W. Coffey, Y. P. Kalmykov, and J. T. Waldron, *The Langevin Equation—With Applications in Physics, Chemistry and Electrical Engineering* (World Scientific, Singapore, 1996).

[191] *NIST Digital Library of Mathematical Functions*, edited by F. W. J. Olver, A. B. Olde Daalhuis, D. W. Lozier, B. I. Schneider, R. F. Boisvert, C. W. Clark, B. R. Miller, B. V. Saunders, H. S. Cohl, and M. A. McClain, Release 1.2.4 (2025), https://dlmf.nist.gov/.

[192] Y. A. Kuznetsov, Practical computation of normal forms on center manifolds at degenerate Bogdanov–Takens bifurcations, Int. J. Bifurcat. Chaos **15**, 3535 (2005).

[193] S. Boccaletti, J. Kurths, G. Osipov, D. Valladares, and C. Zhou, The synchronization of chaotic systems, Phys. Rep. **366**, 1 (2002).

[194] L. M. Pecora and T. L. Carroll, Synchronization in chaotic systems, Phys. Rev. Lett. **64**, 821 (1990).

[195] C. Grebogi, E. Ott, and J. A. Yorke, Chaotic attractors in crisis, Phys. Rev. Lett. **48**, 1507 (1982).

[196] C. Grebogi, E. Ott, and J. A. Yorke, Crises, sudden changes in chaotic attractors, and transient chaos, Physica D **7**, 181 (1983).

[197] C. Grebogi, E. Ott, and J. A. Yorke, Chaos, strange attractors, and fractal basin boundaries in nonlinear dynamics, Science **238**, 632 (1987).

[198] M. W. Beims and J. A. C. Gallas, Alignment of Lyapunov vectors: A quantitative criterion to predict catastrophes? Sci. Rep. **6**, 37102 (2016).

[199] A. Tantet, V. Lucarini, and H. A. Dijkstra, Resonances in a chaotic attractor crisis of the Lorenz flow, J. Stat. Phys. **170**, 584 (2018).

[200] O. Castejón, A. Guillamon, and G. Huguet, Phase-amplitude response functions for transient-state stimuli, J. Math. Neurosci. **3**, 13 (2013).

[201] E. Freire, A. Gasull, and A. Guillamon, Limit cycles and Lie symmetries, Bull. Sci. Math. **131**, 501 (2007).

[202] A. Tantet, M. D. Chekroun, H. A. Dijkstra, and J. D. Neelin, Ruelle-pollicott resonances of stochastic systems in reduced state space. Part II: Stochastic Hopf bifurcation, J. Stat. Phys. **179**, 1403 (2020).

[203] A. Tantet, M. D. Chekroun, J. D. Neelin, and H. A. Dijkstra, Ruelle–Pollicott resonances of stochastic systems in reduced state space. Part III: Application to the Cane–Zebiak model of the El Niño–Southern Oscillation, J. Stat. Phys. **179**, 1449 (2020).

[204] M. D. Chekroun, A. Tantet, H. A. Dijkstra, and J. D. Neelin, Ruelle–pollicott resonances of stochastic systems in reduced state space. Part I: Theory, J. Stat. Phys. **179**, 1366 (2020).

[205] S. Shmakov and P. B. Littlewood, Coalescence of limit cycles in the presence of noise, Phys. Rev. E **109**, 024220 (2024).

[206] M. B. Weissman, $1/f$ noise and other slow, nonexponential kinetics in condensed matter, Rev. Mod. Phys. **60**, 537 (1988).

[207] S. Kogan, *Electronic Noise and Fluctuations in Solids* (Cambridge University Press, Cambridge, 1996).